Laser-driven relativistic optics and particle acceleration in ultrathin foils

Prof. Paul McKenna

University of Strathclyde, Glasgow, UK

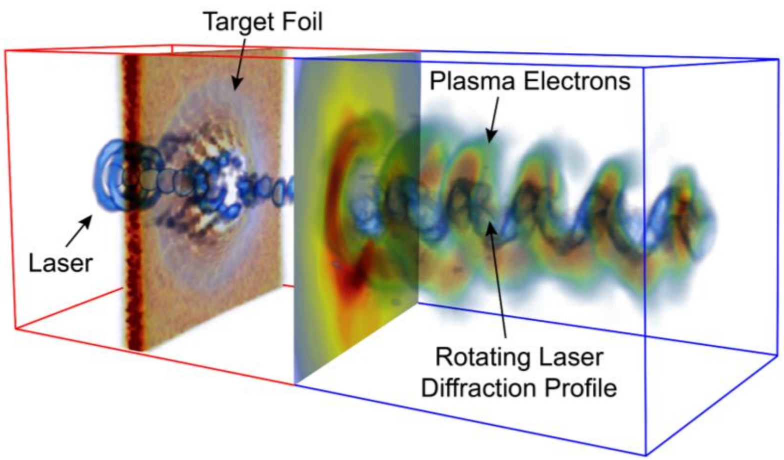

University of Strathclyde, Glasgow

- Founded in 1796 by John Anderson, Professor of Natural Philosophy as ‘a place of useful learning’
- Focus on Science and Engineering
- Became the University of Strathclyde in 1964
- 22,000 students and more than 3,000 staff

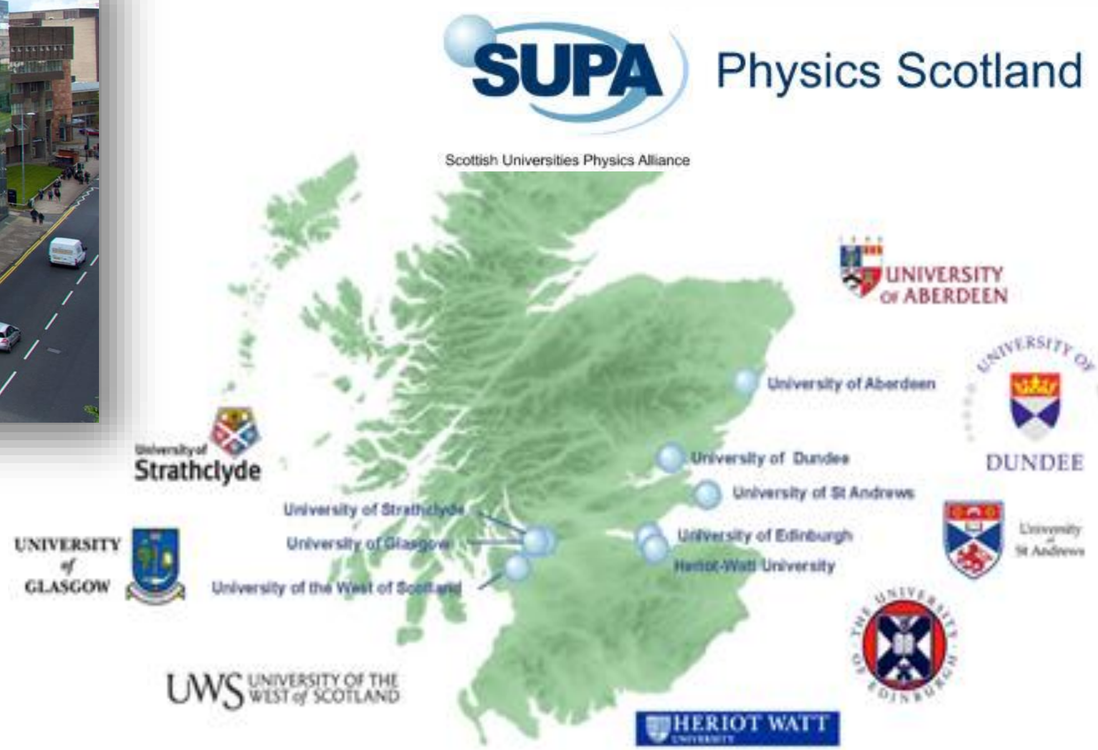

Talk outline

1. Introduction to high power lasers – SCAPA facility
2. Concepts in relativistic laser-plasma physics
3. Overview of our results using PHELIX (since 2010)
4. Laser-driven ion acceleration overview
5. Relativistic plasma aperture formation and laser diffraction
6. Enhancing ion energy via hybrid acceleration schemes

Achievable laser intensity…

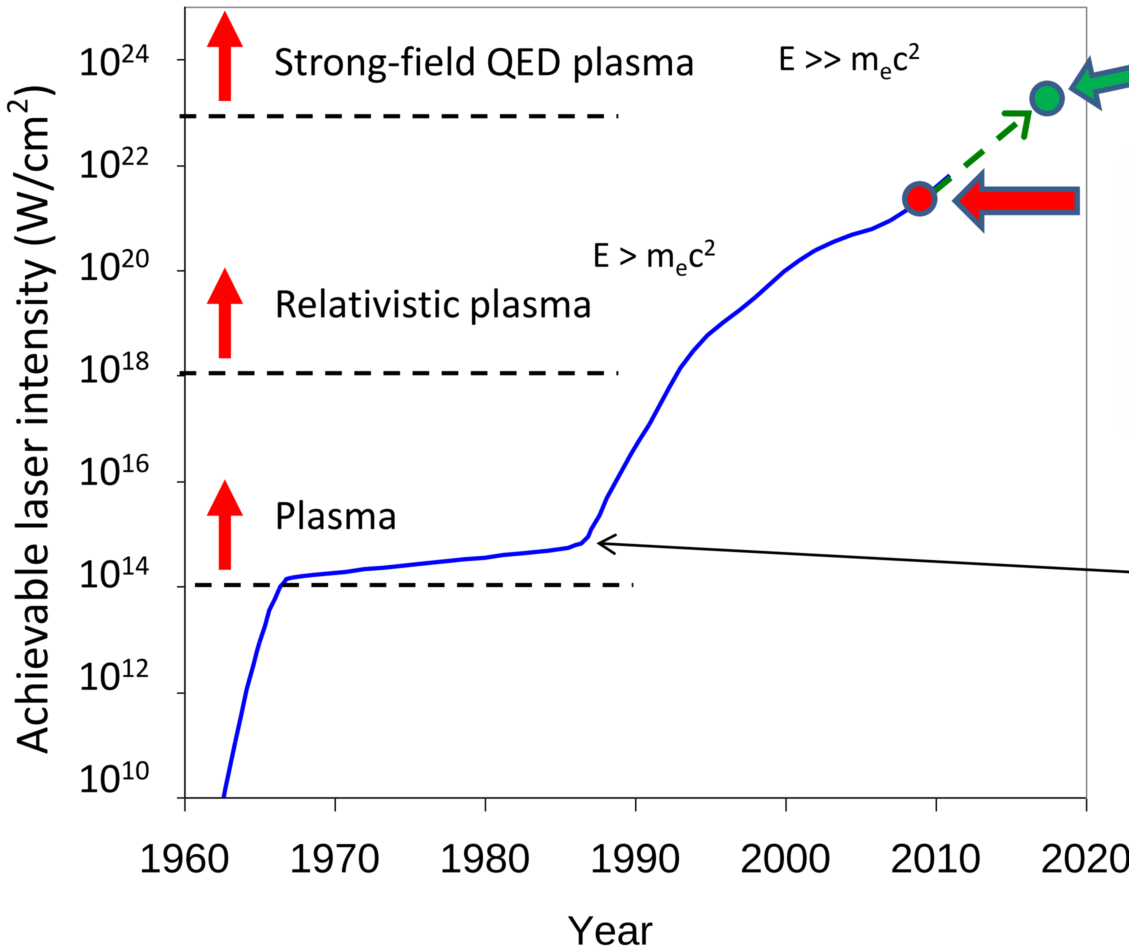

Extreme Light Infrastructure (ELI)

Central Laser Facility, RAL

Phelix, GSI

Chirped pulse amplification (CPA)

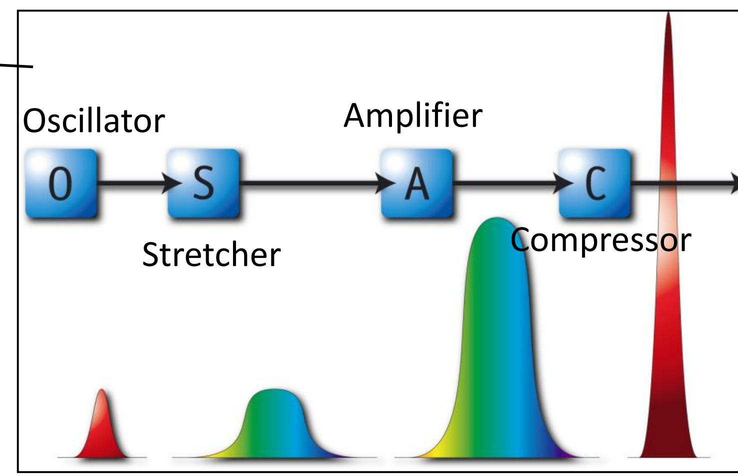

paul.mckenna@strath.ac.uk; GSI-22/05/2018

High power laser facilities worldwide

University of

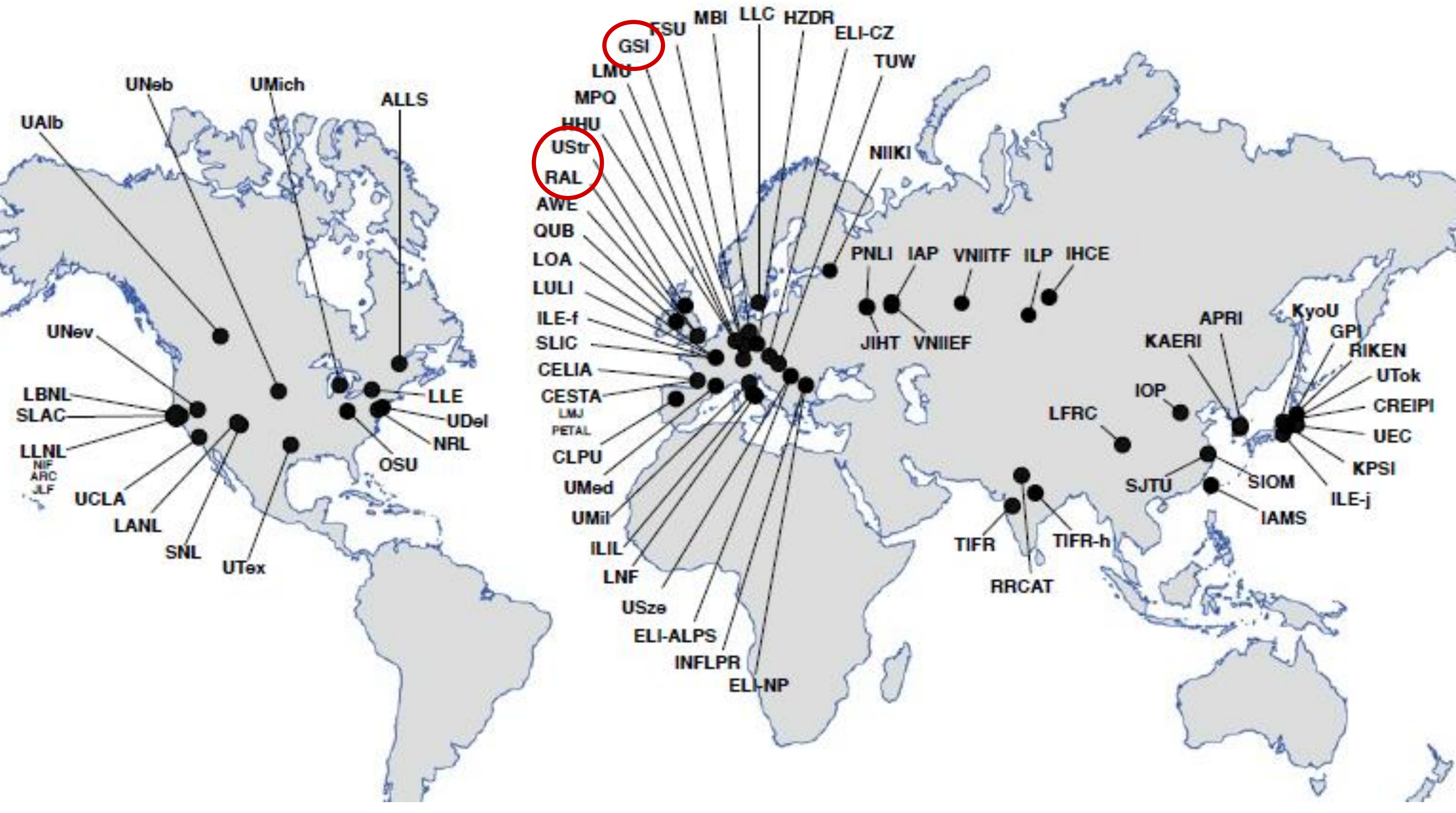

www.ICUIL

SCAPA: Scottish Centre for Applications of Plasma Accelerators

University of Strathclyde Glasgow

- **3 shielded areas** with multiple beam lines.
- High-intensity fs laser systems:
  - a) 350 TW at 5 Hz,
  - b) 40 TW at 10 Hz,
  - c) sub-TW at kHz.
- High-energy **ion and electron** bunches,
- Bbright **X-ray/γ-ray** and **neutron** pulses.

SCAPA 350 TW laser commissioned

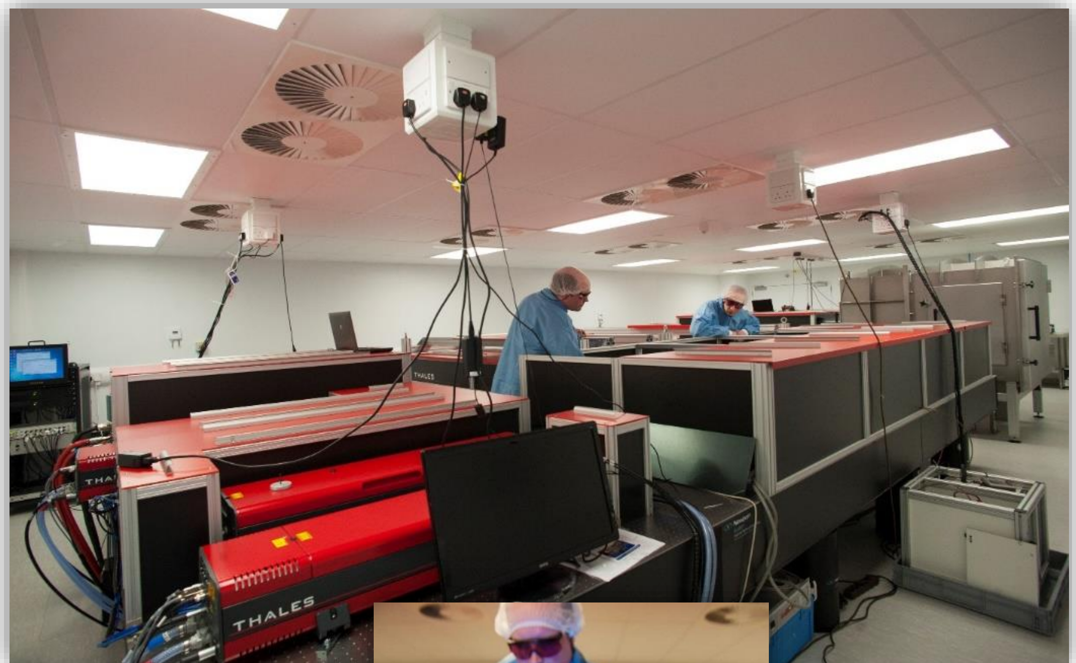

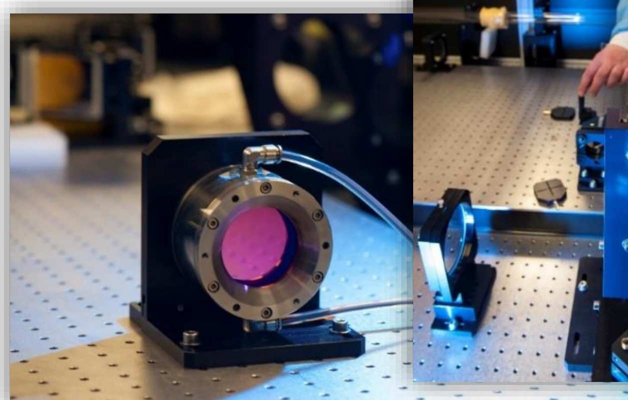

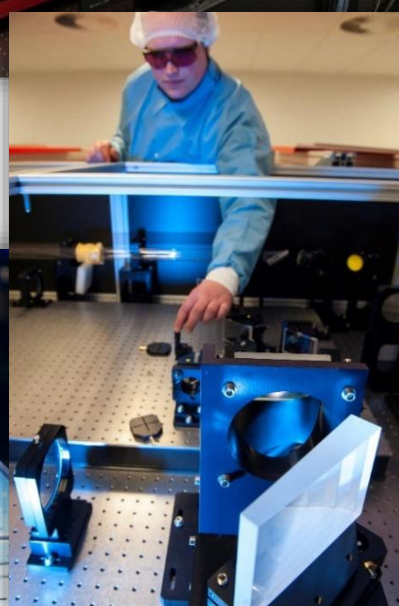

Parameter	Laser Warranted value at 5 Hz
Peak Power	≥350 TW
FWHM pulse duration	≤25 fs
Energy per pulse (after compressor)	≥ 8.75 J
Pulse repetition rate	5 Hz
Contrast ratio	10^{10}:1 @ 100 ps; 10^{8}:1 @ 30 ps; 10^{4}:1 @ 2ps; ASE contrast 10^{10}:1
Short term stability	<1.2% rms (over 500 shots) <1.5% rms (over working day, 8 hours)
Central Wavelength	800 ± 10 nm
Beam quality Strehl ratio	≥0.85
Pointing Stability	<5 μrad
Attenuator	10 – 100 %
Probe beam	30 mJ uncompressed synchronised beam

Collective electron dynamics in laser-plasma

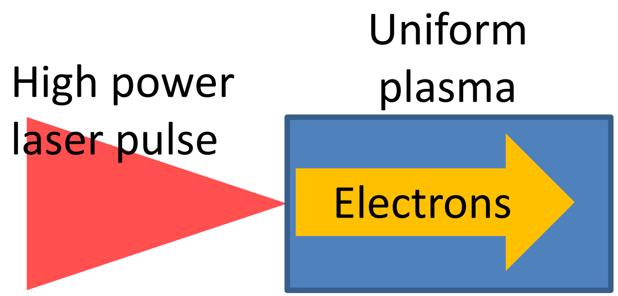

Collective electron dynamics in laser-plasma

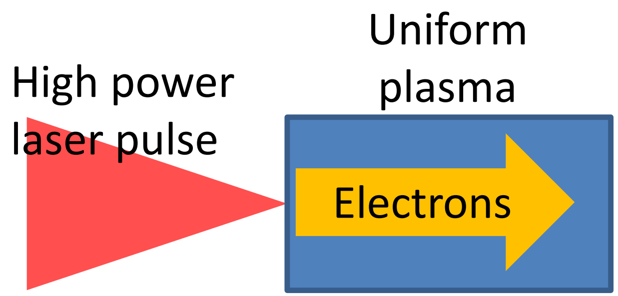

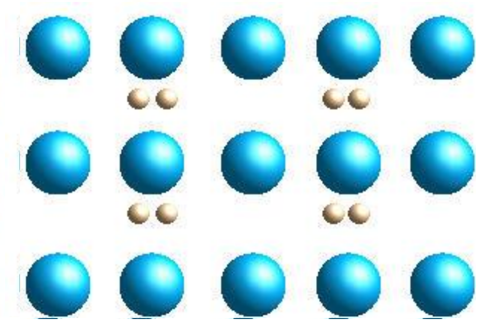

In the interaction of a laser pulse with plasma, electrons collectively quiver around the (almost) stationary ions
$\Rightarrow$ plasma oscillations

Electron plasma frequency:

$$\omega_{\text{plasma}} = \sqrt{\frac{e^2}{\varepsilon_0}\frac{n_e}{m_e}}$$

n_e ← Electron density

m_e ← Electron mass

If $\omega_{\text{plasma}} > \omega_{\text{(Laser)}}$ the plasma electrons can follow the light oscillations and therefore cancel the light propagation.

paul.mckenna@strath.ac.uk; GSI-22/05/2018

Relativistic non-linear optics

Electron mass increase by the relativistic factor $\gamma = \frac{1}{\sqrt{1 - v^2/c^2}}$

Relativistic Self-Focussing

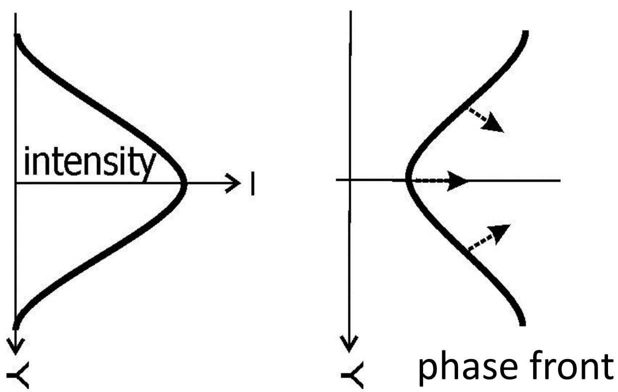

- Refractive index $n = \sqrt{1 - \frac{\omega_p^2/<\gamma>}{\omega_{Las}^2}}$
- phase velocity $v_{ph}=c/n$ is smaller on-axis
- plasma acts like a positive lens - self-focusing for powers beyond critical level.

Relativistic Induced Transparency

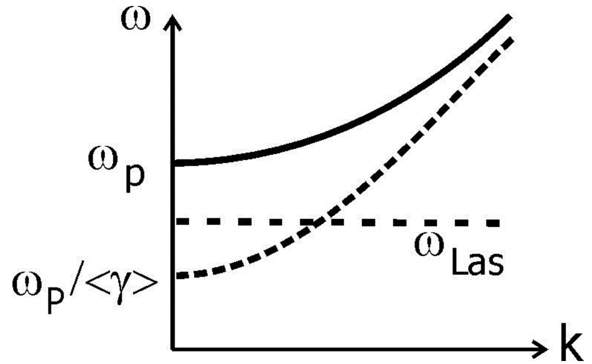

- In dense plasma with $\omega_p > \omega_{Las}$, light cannot propagate
- The dispersion relation governing laser light propagation depends on plasma frequency $\omega_p^2=4\pi e^2 n_e/m$ and the average $<\gamma>$-factor.
- Plasma becomes transparent for large $<\gamma>$

Collective electron dynamics in laser-plasma

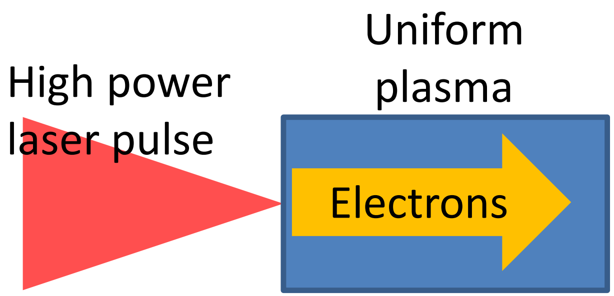

Gas → Solid

$\omega_{\text{plasma}} < \omega_{\text{Laser}}$

Underdense plasma

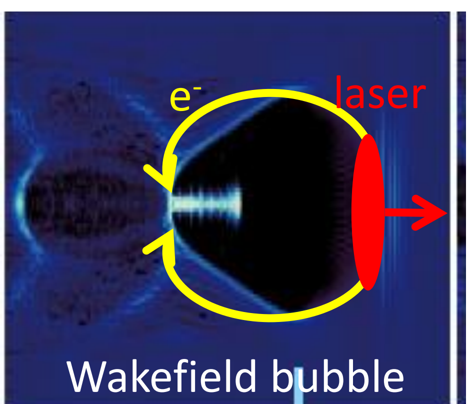

Wakefield electron acceleration

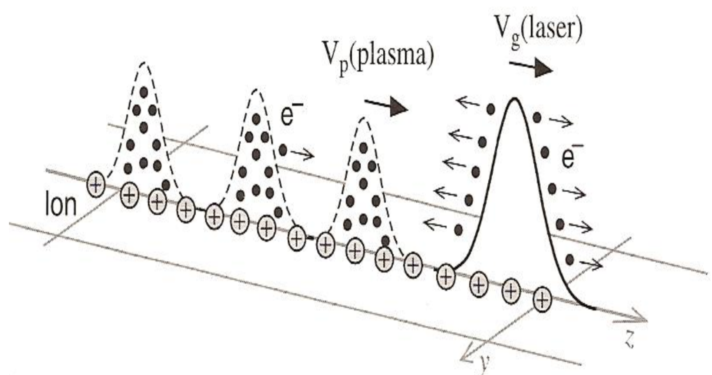

paul.mckenna@strath.ac.uk; GSI-22/05/2018

Collective electron dynamics in laser-plasma

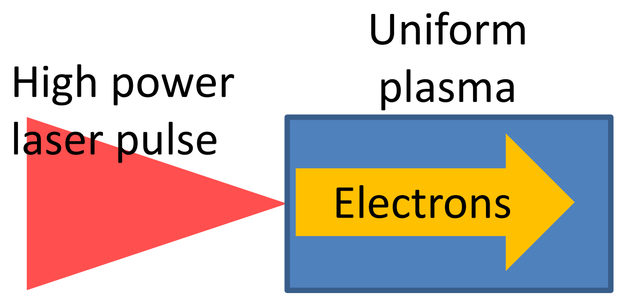

Gas → Solid

$\omega_{\text{plasma}} > \omega_{\text{Laser}}$

Overdense plasma

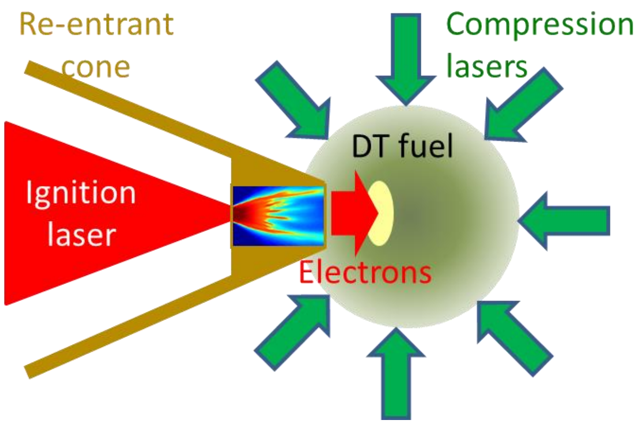

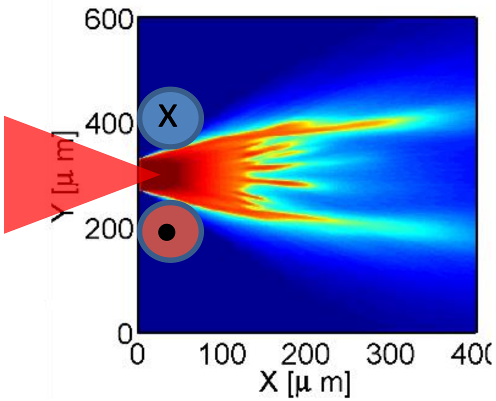

Electron transport e.g. for Fast Ignition ICF

Progress in intense laser-solid interactions

Dual-pulse optimisation

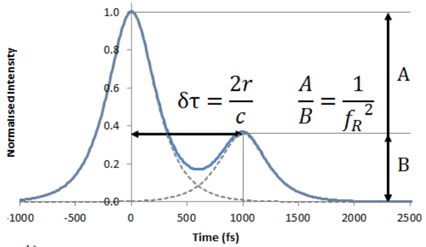

Scott et al App. Phys. Lett., (2012)
Markey et al Phys. Rev Lett., 105, 195008 (2012)

Laser focus effects

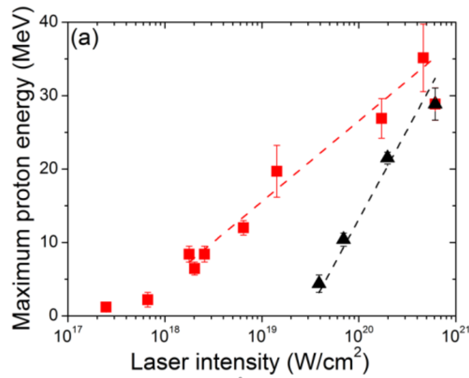

Coury *et al* App. Phys. Lett., **100**, 074105 (2012) & Brenner et al LPB (2012)

Mass-limited targets

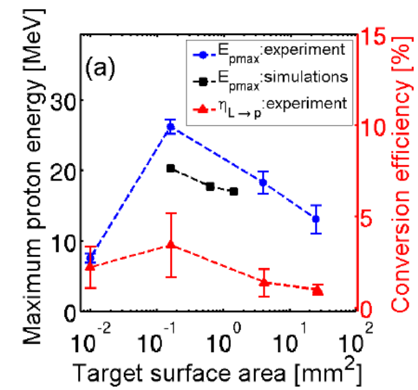

Tresca *et al* PPCF 53, 105008 (2011)
Gray *et al* App. Phys. Lett, 99, 171502 (2011)

Optimum density gradients

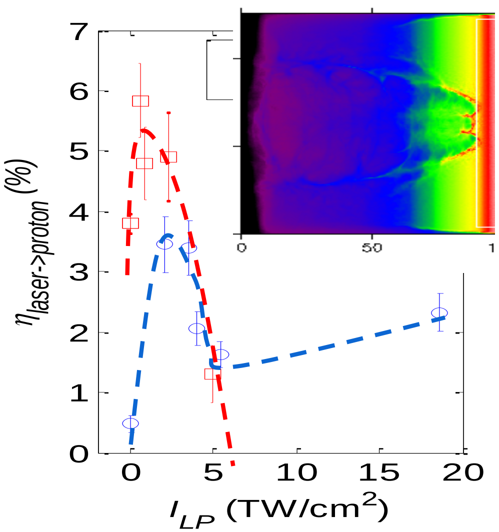

McKenna *et al* LPB, **12,** 045018 (2010)
Gray et al, New J. Physics (2014)

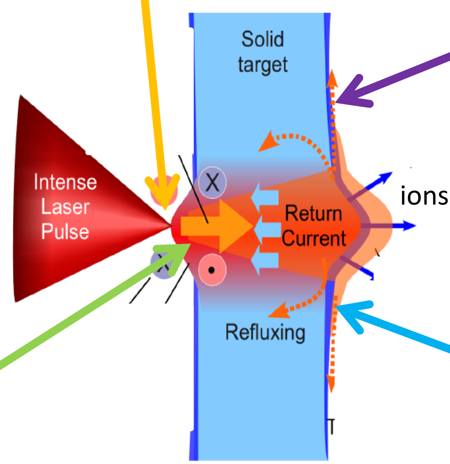

'Shaping' the ion beam

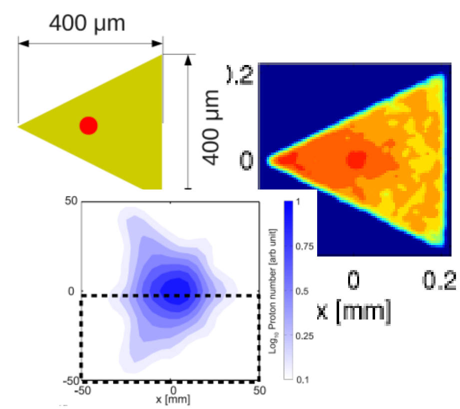

Tresca et al PPCF 53, 105008 (2011)

Progress in intense laser-solid interactions

Role of lattice structure in the resistivity of transient Warm Dense Matter and electron transport

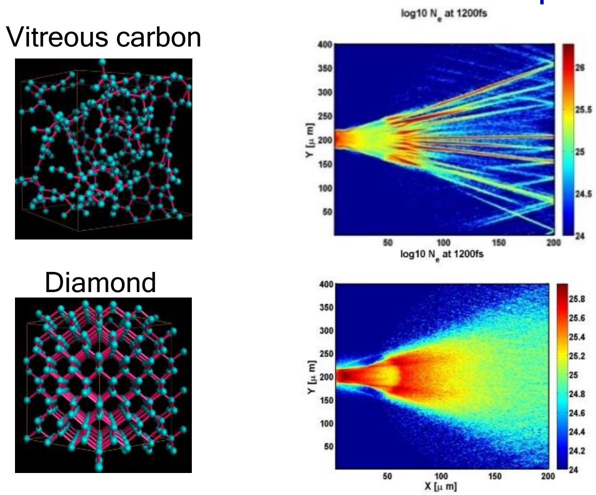

McKenna *et al*, Phys. Rev. Lett. 106, 184004 (2011)
McKenna *et al*, Plas. Phys. Cont. Fus. 57, 064001(2015)

Manipulating fast electron transport via self-generated resistive magnetic fields

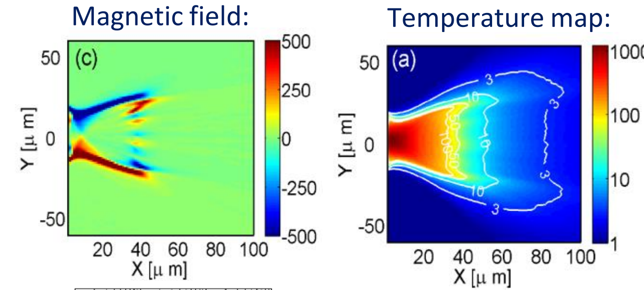

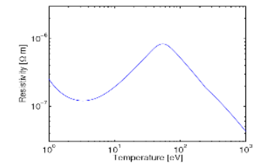

$$\frac{\partial \mathbf{B}}{\partial t} = \eta \nabla \times \mathbf{j}_f + (\nabla \eta) \times \mathbf{j}_f$$

MacLellan et al, Phys. Rev. Lett. 111, 095001 (2013)
MacLellan et al, Phys. Rev. Lett., 113 185001 (2014)
R. J. Dance, et al., Plas. Phys. Cont. Fus, 58, 014027 (2016)

Fast electron recirculation

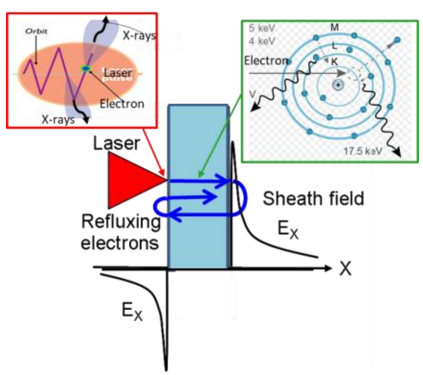

Yuan et al, New J. Phys. 12, 063018 (2010)
Quinn et al, PPCF, 53, 025007 (2011)
Gray et al, New J. Phys. 20, 033021 (2018)

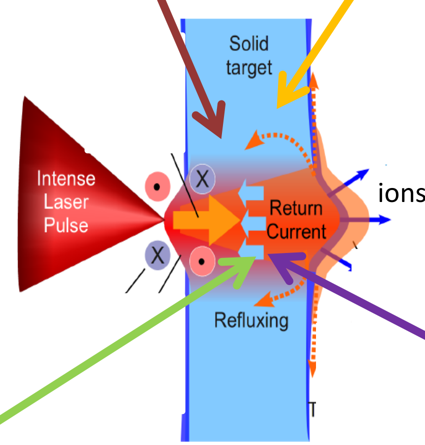

Lateral fast electron transport

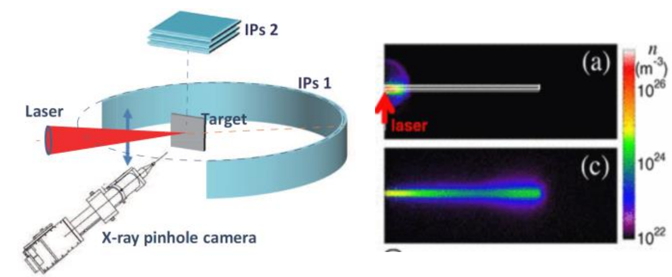

McKenna, et al., Phys. Rev. Lett. 98, 145001 (2007)
Ge *et al* App. Phys. Lett, 107, 091111 (2015)

Total energy absorption studies using Phelix

Gray et al, New J. Phys. 20, 033021 (2018)

- Large volume Ulbricht sphere developed
- Used to investigate laser energy absorption as a function of laser and target properties

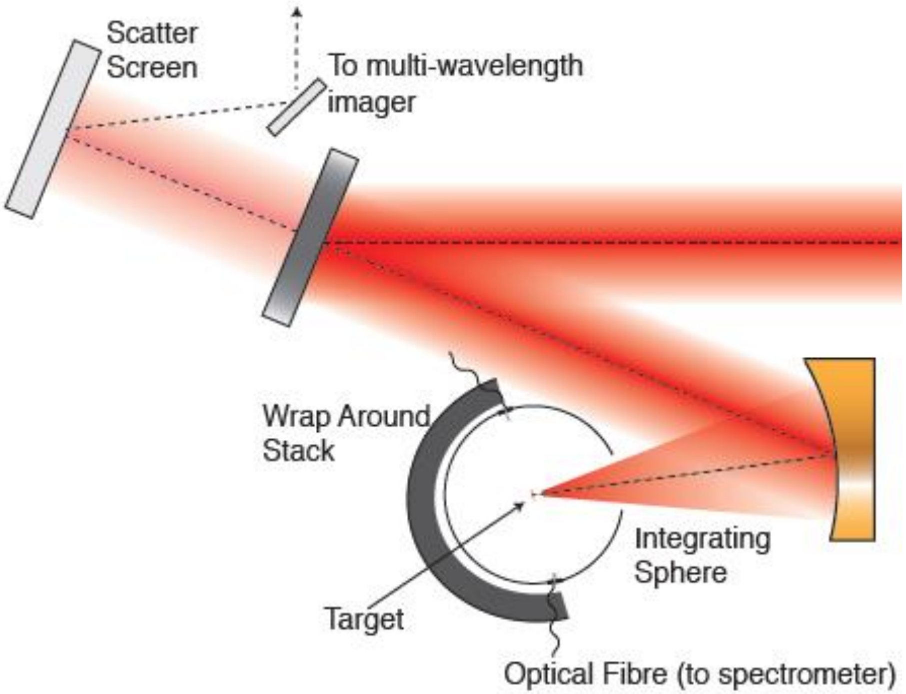

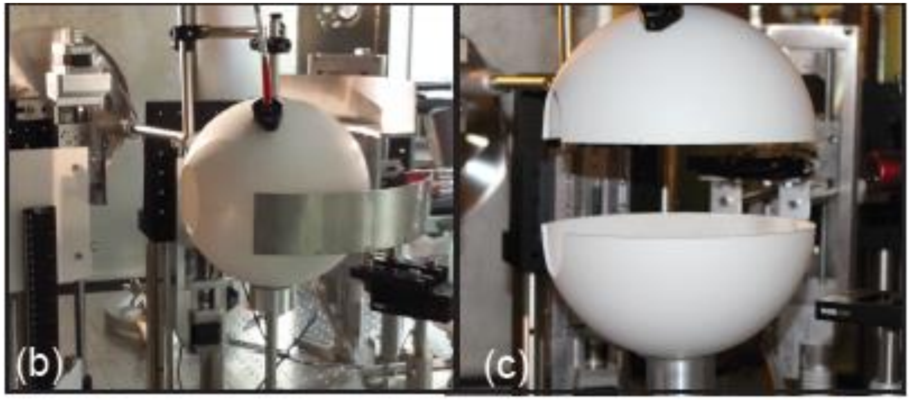

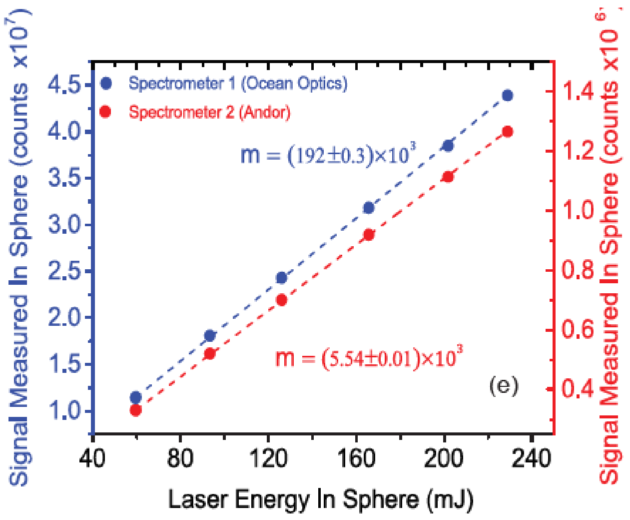

Total energy absorption studies using Phelix

Gray et al, New J. Phys. 20, 033021 (2018)

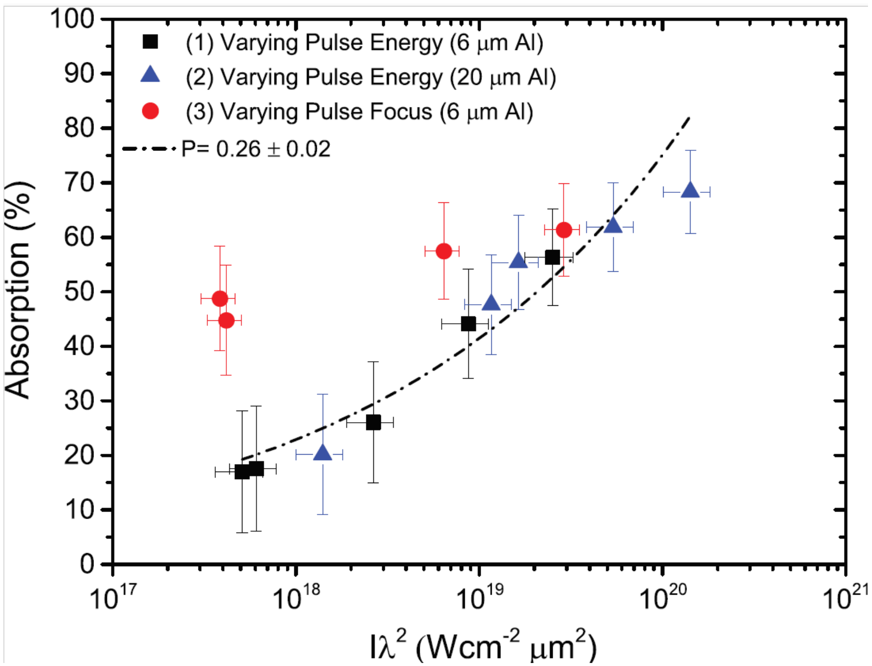

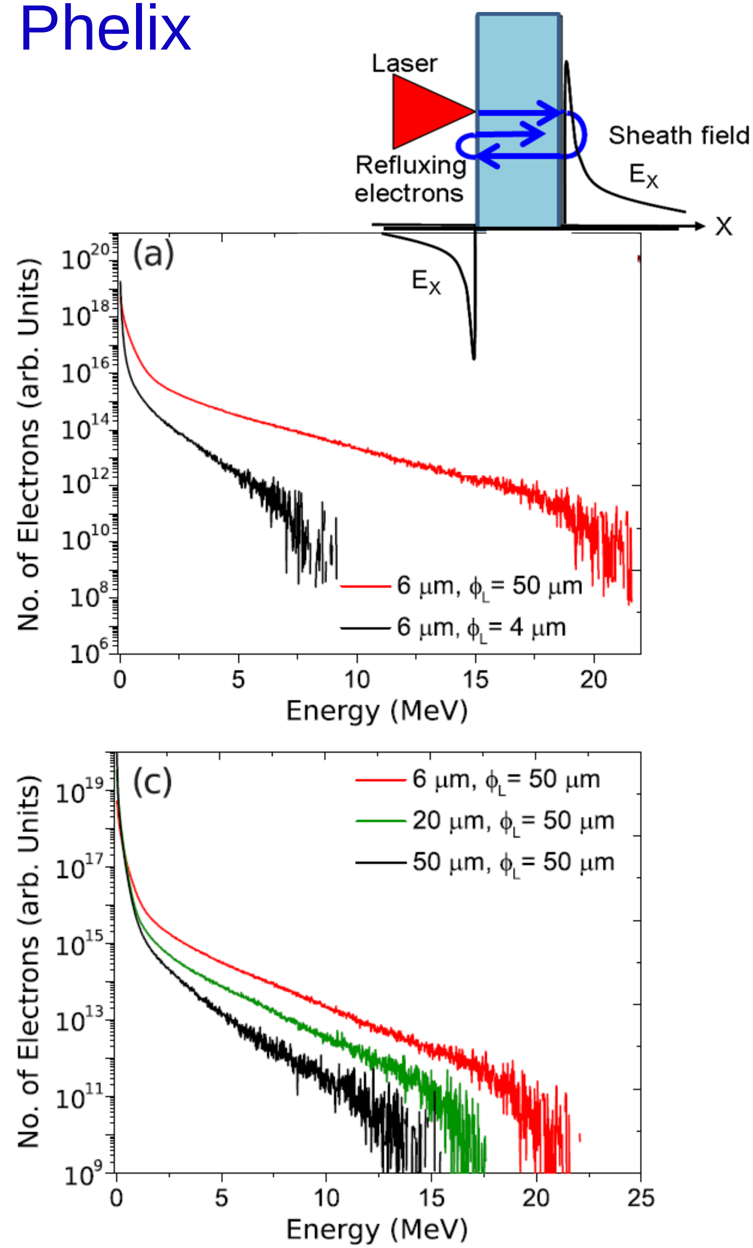

- Different scaling with intensity measured when focal spot is varied as opposed to pulse energy
- EPOCH PIC simulations and analytical modelling shows that absorption is enhanced when significant fast electron refluxing occurs within the target

Weibel instability in ion acceleration using Phelix

G. Scott *et al*, New Journal of Physics, 19, 043010 (2017)

Onset of Weibel instability in expanding dense plasma Investigated using a double laser pulse (pump-probe) scheme

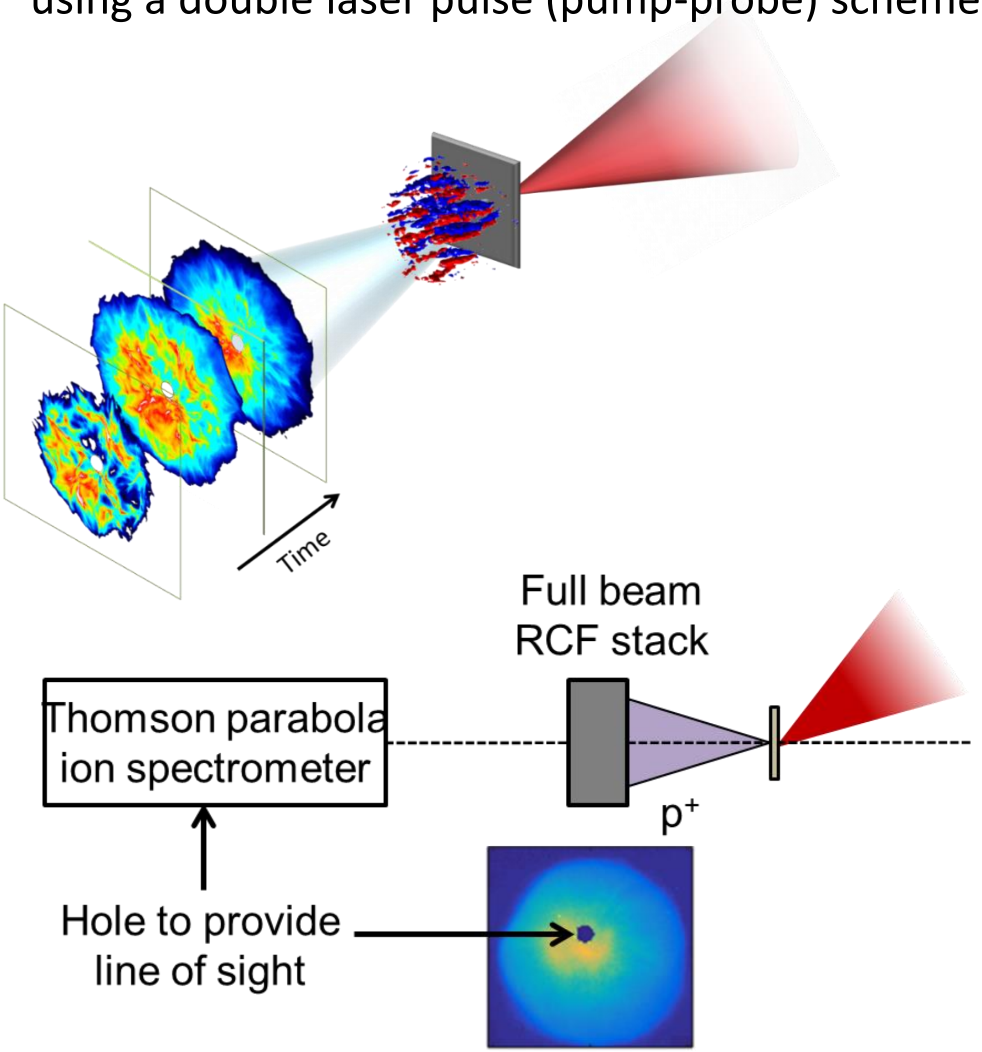

- Double pulse configuration used
- Prepulse to main pulse energy ratio: 1:10
- Total laser energy on target: 72 ± 2 J
- Time between pulses: 1-100 ps
- Main pulse intensity: 4×10^{18} Wcm^{-2}

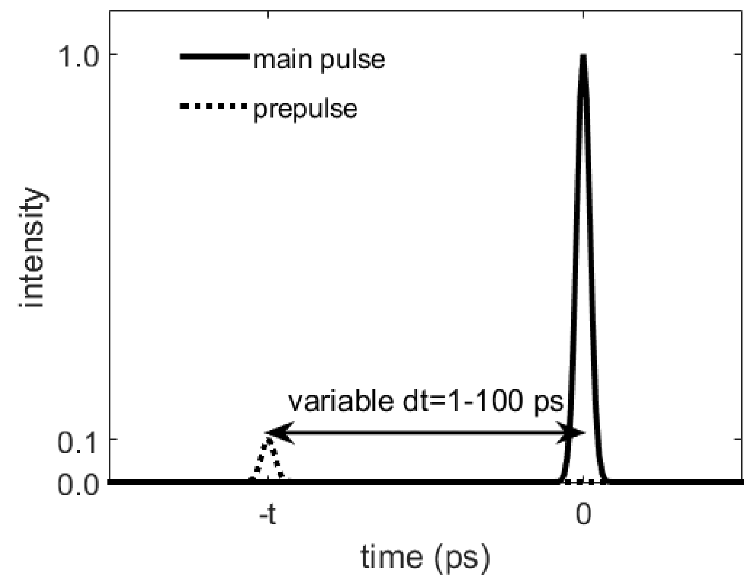

Weibel instability in ion acceleration using Phelix

G. Scott *et al*, New Journal of Physics, 19, 043010 (2017)

Spatial-intensity distribution of sheath-accelerated proton beam is modulated due to Weibel instability in preplasma at target foil rear surface

Fundamental plasma physics interest and imposes constraints on the preplasma levels tolerated for high quality proton acceleration

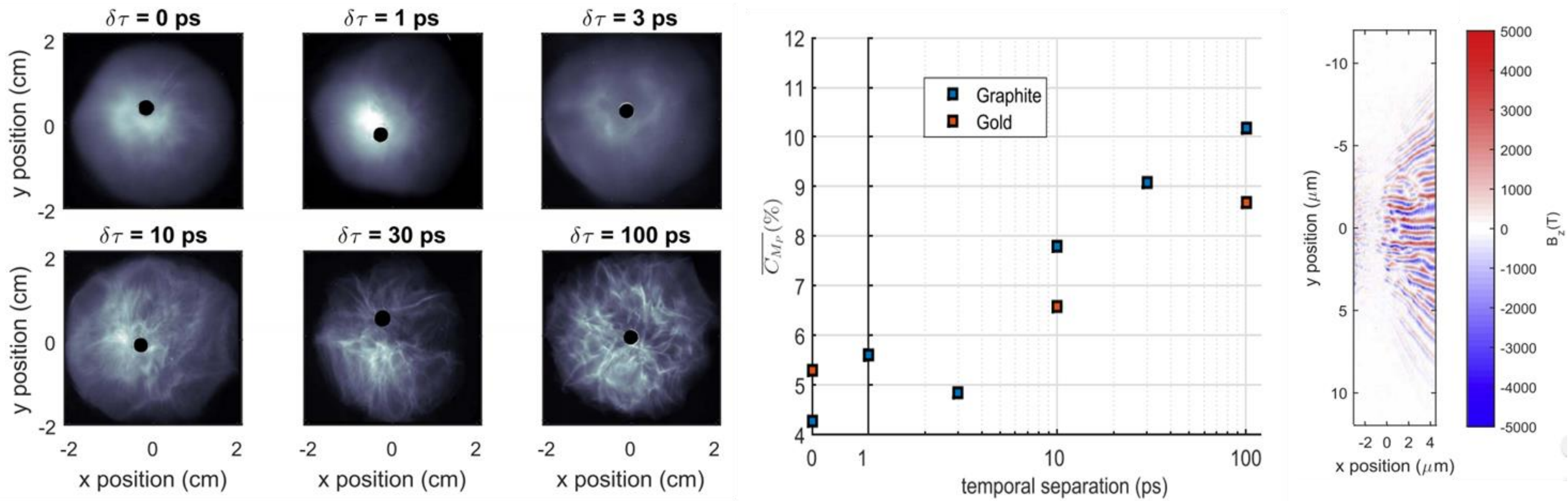

Weibel instability growth with increase plasma expansion (increasing temporal separation)

Strathclyde publications from Phelix experiments 2011-18

1. Escaping electrons from intense laser-solid interactions as a function of laser spot size, Rusby et al., **Euro. Phys. Journal** 167, 02001 (2018)
2. Enhanced laser-energy coupling to dense plasmas driven by recirculating electron currents, Gray et al., **New J. Phys.** 13 (2018)
3. Diagnosis of Weibel instability evolution in the rear surface scale lengths of laser solid interactions via proton acceleration, Scott, et al., **New J. Phys.** 19, 043010 (2017)
4. Role of lattice structure and low temperature resistivity on fast electron beam filamentation in carbon, Dance et al., **Plasma Phys. Control. Fusion.** 58, 014027, (2015)
5. Measurement of the angle, temperature and flux of fast electrons emitted from intense laser-solid interactions, Rusby et al., **J. Plasma Phys**. 81, 5, 9 p., 475810505, (2015)
6. Directed fast electron beams in ultraintense picosecond laser irradiated solid targets, Ge et al., **Appl. Phys. Lett.**. 107, 9, 5 p., 091111, (2015)
7. Optimisation of plasma mirror reflectivity and optical quality using double laser pulses, Scott et al., **New J. Phys.** 16 (2015)
8. The influence of preformed plasma on the surface-guided lateral transport of energetic electrons in ultraintense short laser-foil interactions, Yuan et al., **Plasma Phys**. **Cont**. **Fus.** 56, 055001, (2014)
9. Multi-pulse enhanced laser ion acceleration using plasma half cavity targets, Scott et al., **Appl. Phys. Lett.**, 101, 024101 (2012)
10. Surface Transport of Energetic Electrons in Intense Picosecond Laser-Foil Interactions, Gray et al., **Appl. Phys. Lett.**, 99, 171502 (2011)
11. Spatially resolved X-ray spectroscopy using a flat HOPG crystal, Yuan et al., **Nucl. Instrum. Methods A**, 653 (1). pp. 145-149 (2011)
12. Controlling the properties of ultraintense laser–proton sources using transverse refluxing of hot electrons in shaped mass-limited targets, Tresca et al., **Plasma Phys. Cont. Fus.** 53, 105008 (2011)
13. Refluxing of fast electrons in solid targets irradiated by intense, picosecond laser pulses, Quinn et al., **Plasma Phys. Cont. Fus.** 53, 025007 (2011)

Collective electron dynamics in laser-plasma

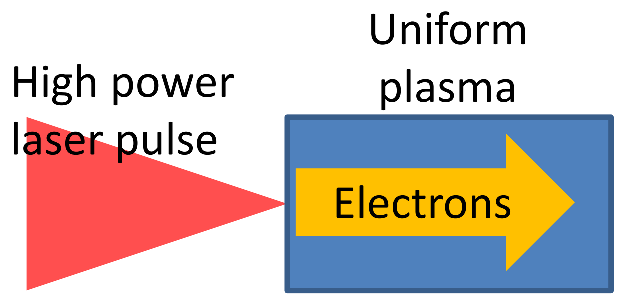

Gas → Solid

$\omega_{\text{plasma}} < \omega_{\text{Laser}}$

Underdense plasma

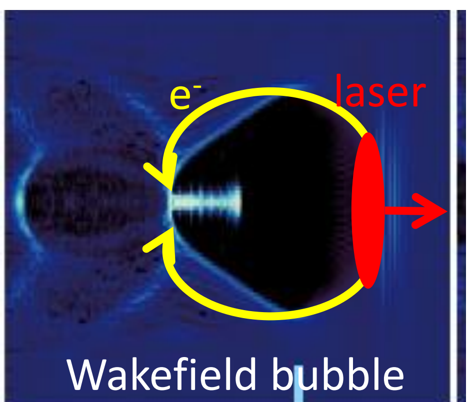

Wakefield electron acceleration

$\omega_{\text{plasma}} > \omega_{\text{Laser}}$

Overdense plasma

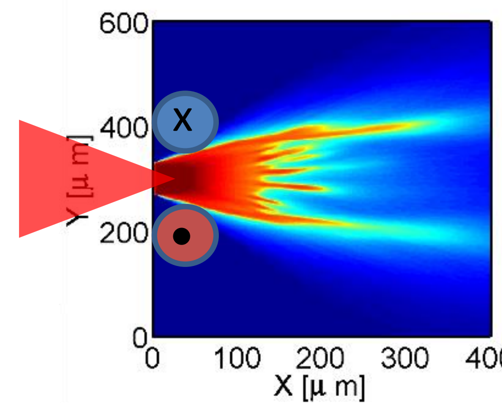

Electron transport e.g. for Fast Ignition ICF

Collective electron dynamics in laser-plasma

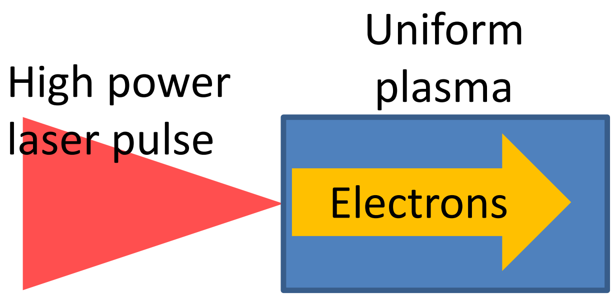

Gas → Solid

$\omega_{\text{plasma}} < \omega_{\text{Laser}}$

Underdense plasma

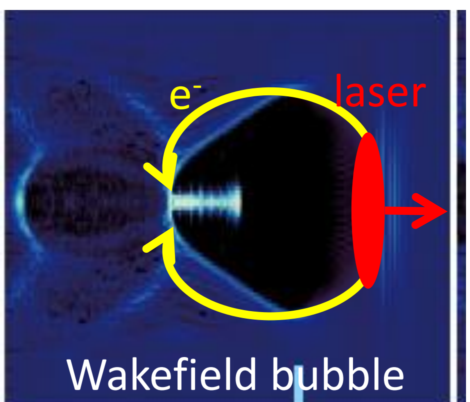

Wakefield electron acceleration

$\omega_{\text{plasma}} \sim \omega_{\text{Laser}}$

Foils expanding to near critical density plasma

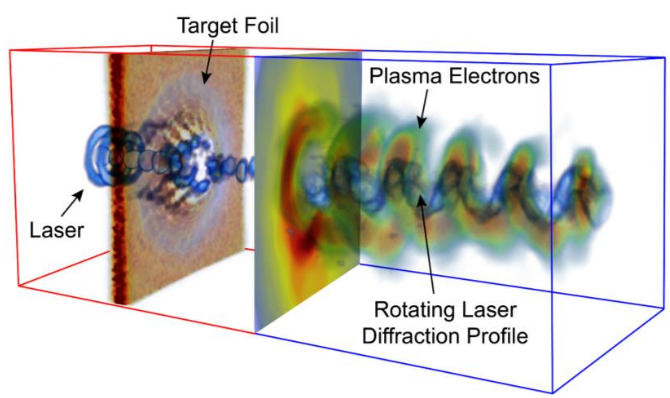

Ion acceleration and HHG

$\omega_{\text{plasma}} > \omega_{\text{Laser}}$

Overdense plasma

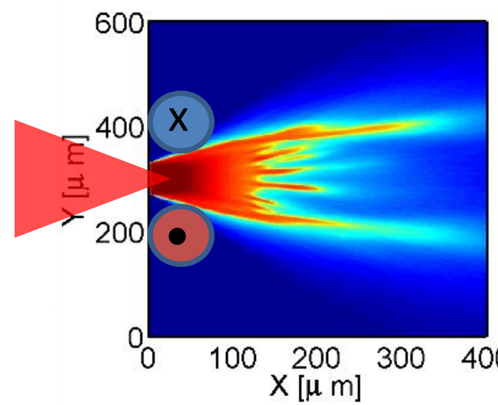

Electron transport e.g. for Fast Ignition ICF

Laser-ion acceleration mechanisms

Numerous acceleration mechanisms have been identified, in overdense, underdense and near critical density targets

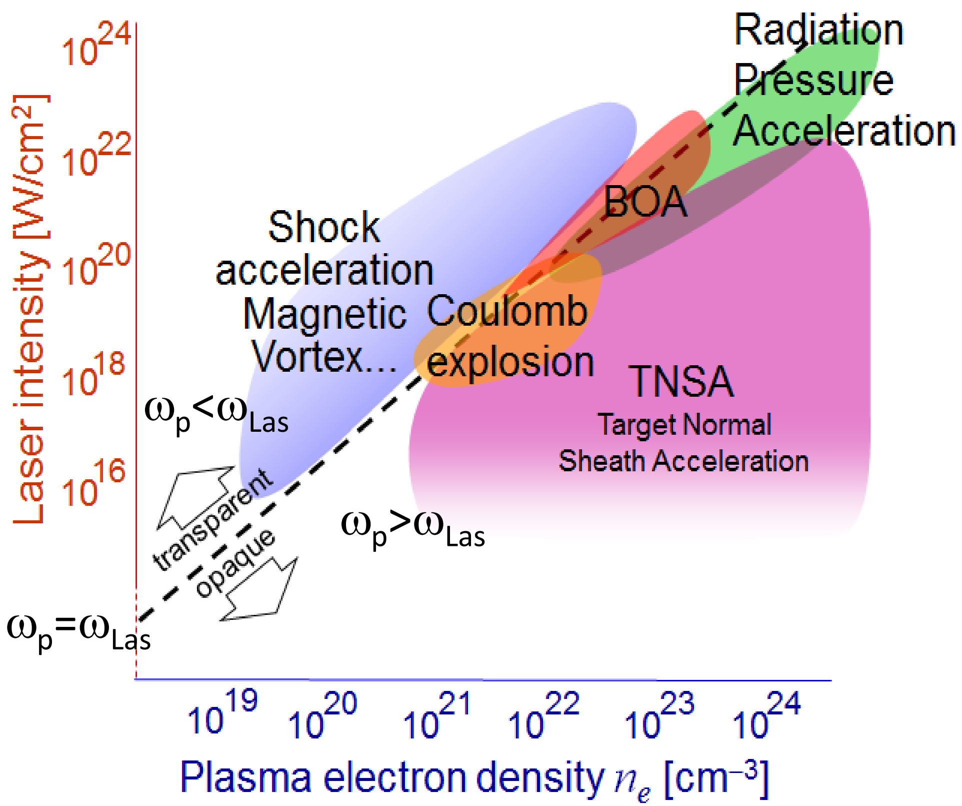

Laser-ion acceleration mechanisms

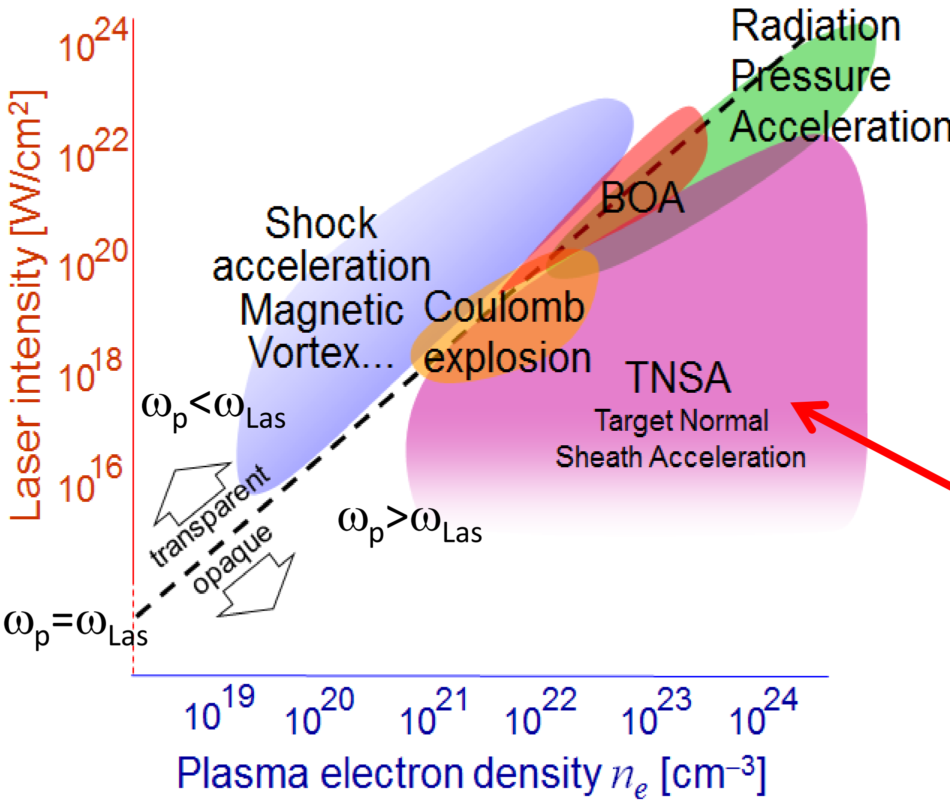

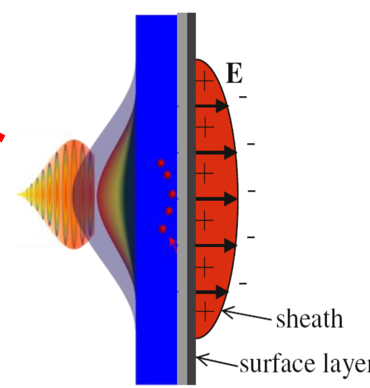

Ion acceleration

General features of Target Normal Sheath Acceleration

Sheath field established on foil surface

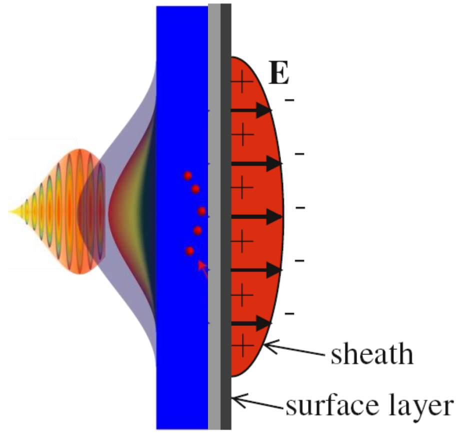

Broad energy spectrum of ions

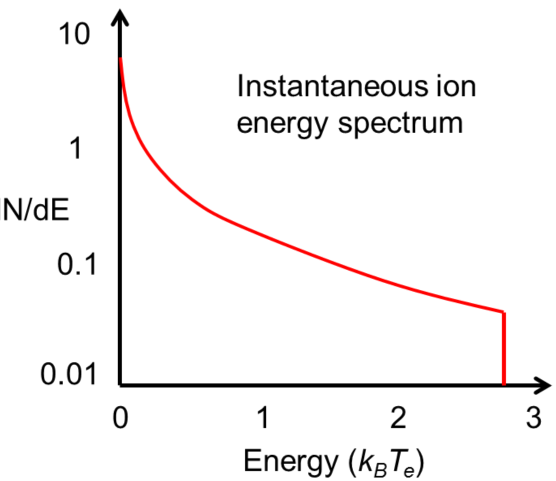

Plasma expansion dynamics

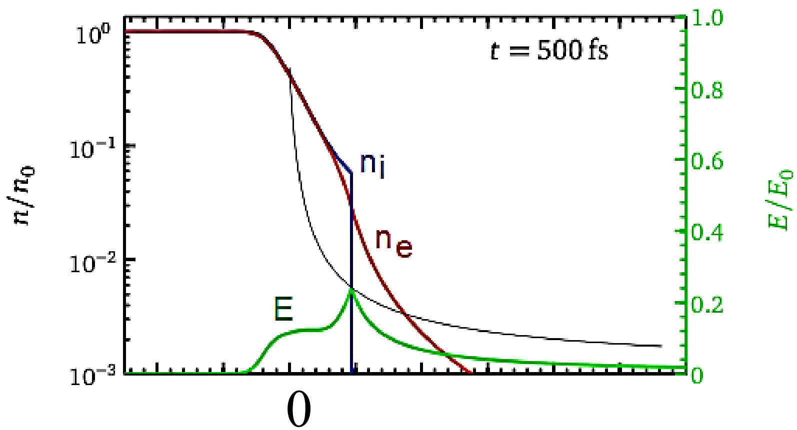

Divergence decreases with increasing ion energy

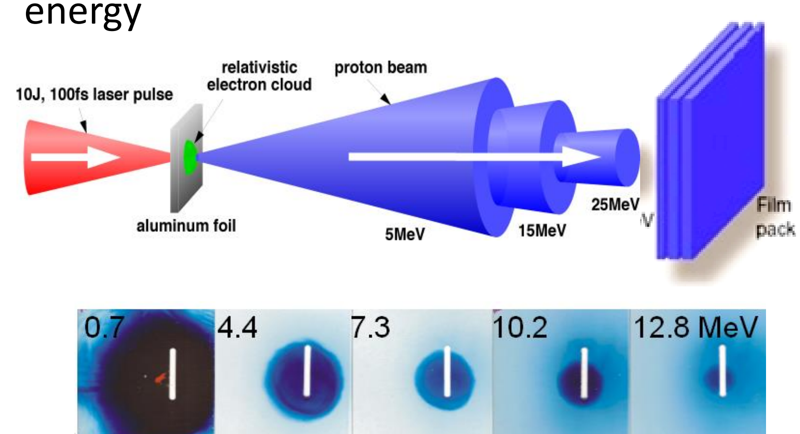

Laser-ion acceleration mechanisms

At high enough intensity, radiation pressure drives plasma surface inwards: Hole Boring

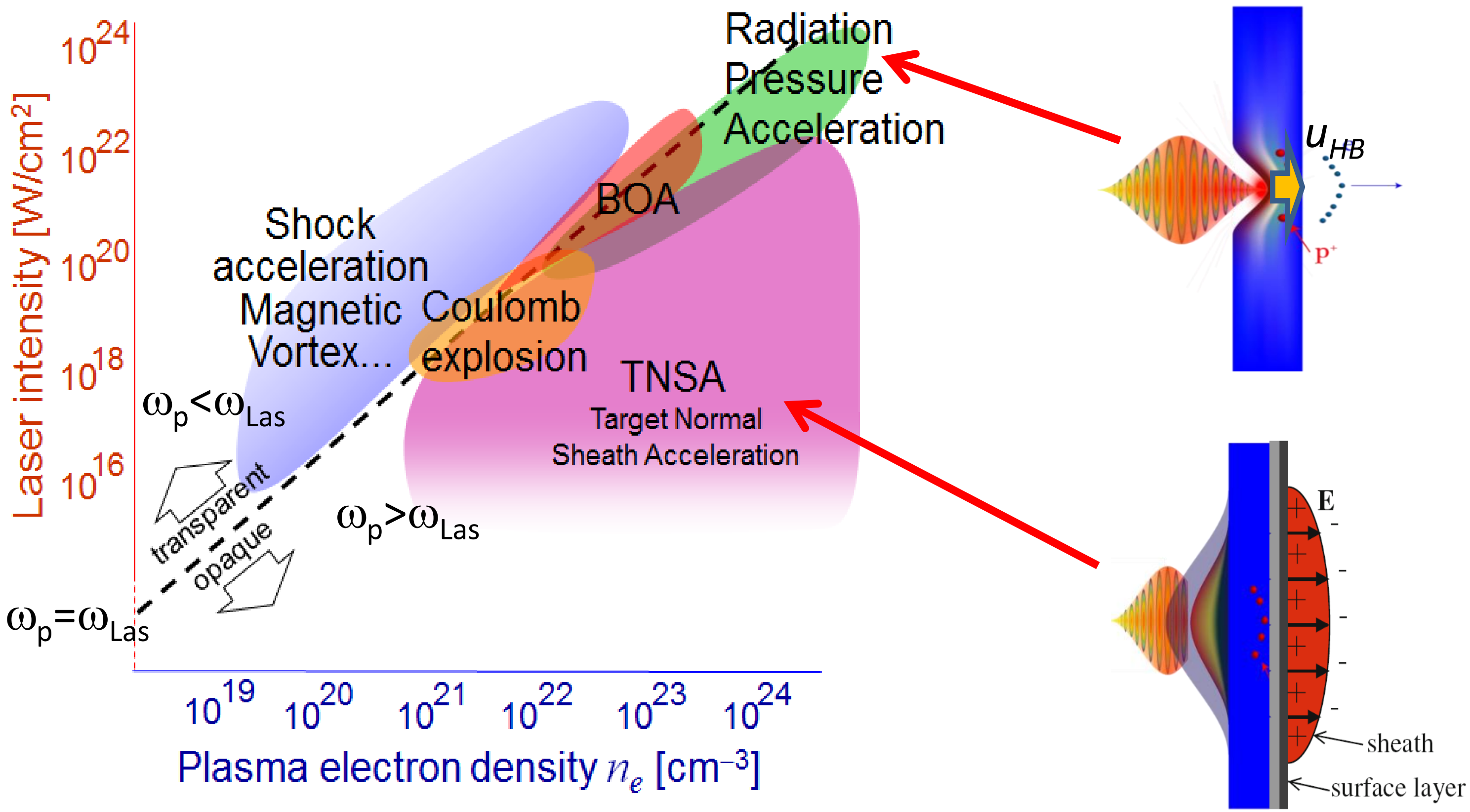

Laser radiation pressure acceleration

Radiation pressure via Photons

Photon flux (no. of photons per sec per unit area; units $cm^{-2}s^{-1}$): $F_{ph} = \frac{I_L}{\hbar\omega_L}$

Momentum flux or Pressure (force per unit surface): $P_{rad} = \hbar k F_{ph} = \frac{I_L k}{\omega_L}$

The laser ponderomotive force pushes and piles up electrons in the skin layer creating a static field that acts on the ions.

Results in an ion population with energy per nucleon equal to:

$$\varepsilon_{HB} = \frac{m_p}{2}(2u_{HB})^2 = \frac{2m_p I_L}{\rho c}$$

$$= 2m_e c^2 \frac{Zn_c}{An_e} a_0^2$$

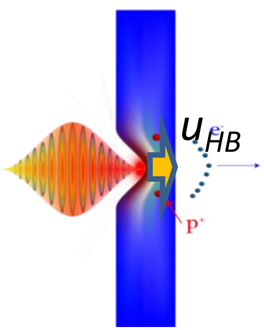

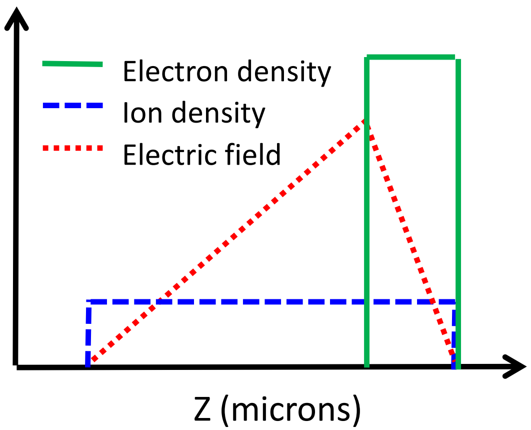

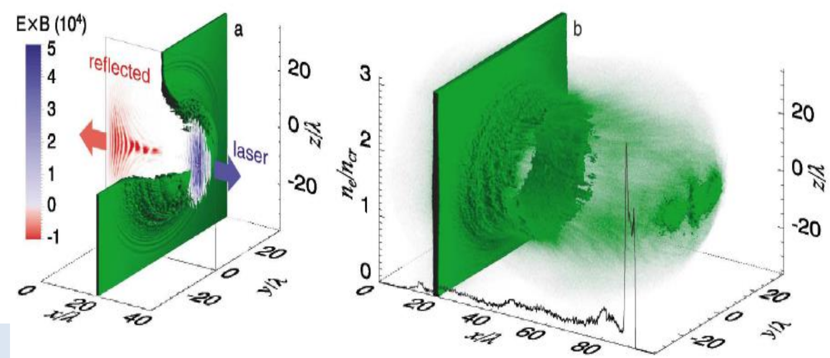

T. Esirkepov, *et al.,* PRL. **92,** 175003 (2004)

Predicted beam properties:

- Fast scaling with laser intensity
- Narrow-band spectrum (whole-foil acceleration)
- Narrow divergence (assuming large focal spot)

Relativistic transparency enhanced acceleration

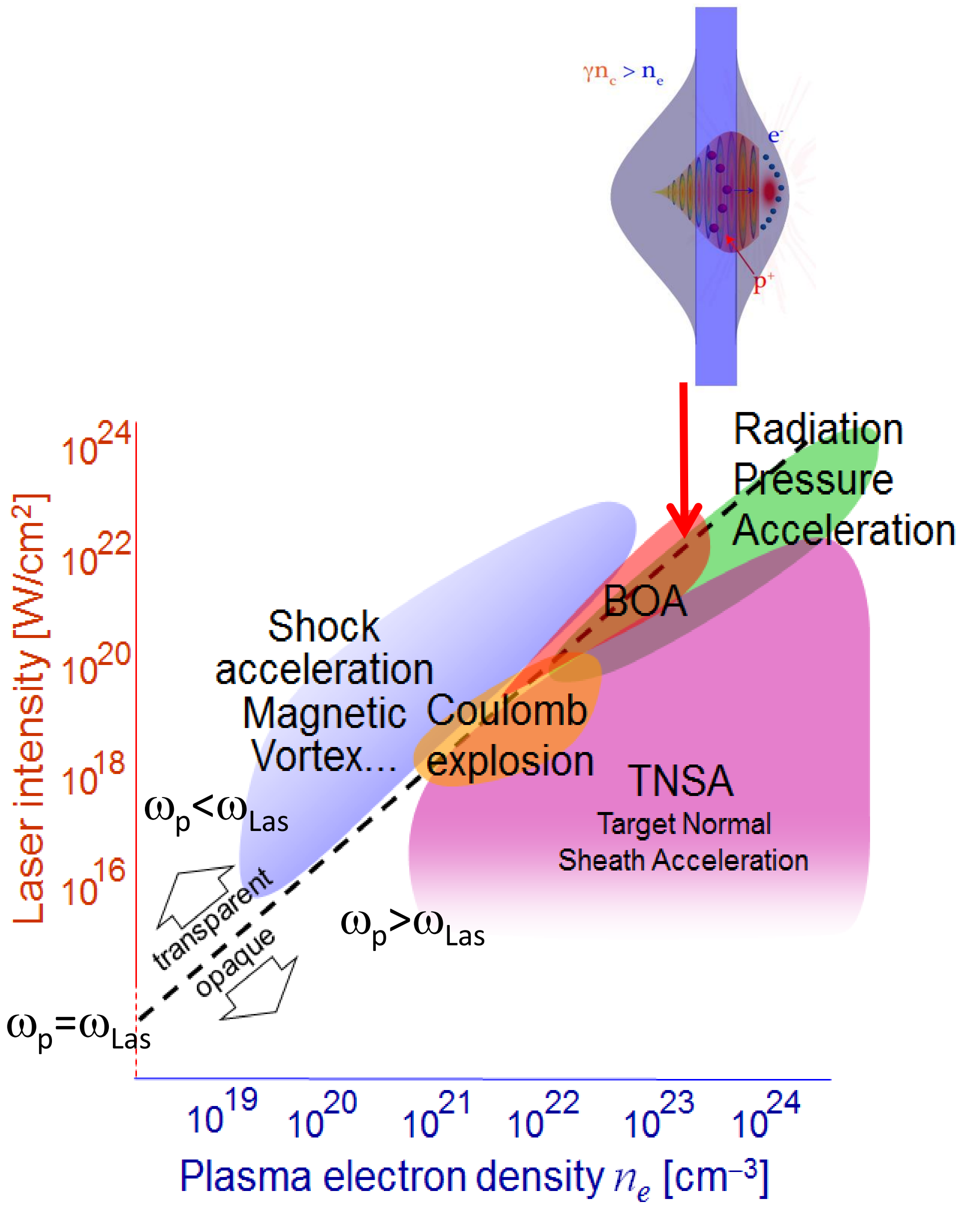

Plasma frequency: $\omega_p = \sqrt{\dfrac{e^2}{\varepsilon_0}\dfrac{n_e}{m_e}}$

Transparency when $\omega_p < \omega_L$

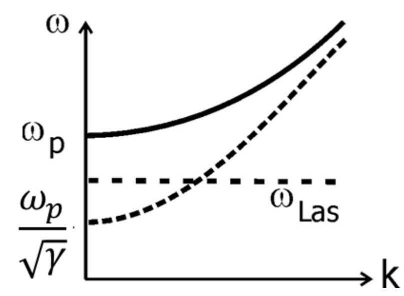

3D PIC simulations with a uniform planar target foil

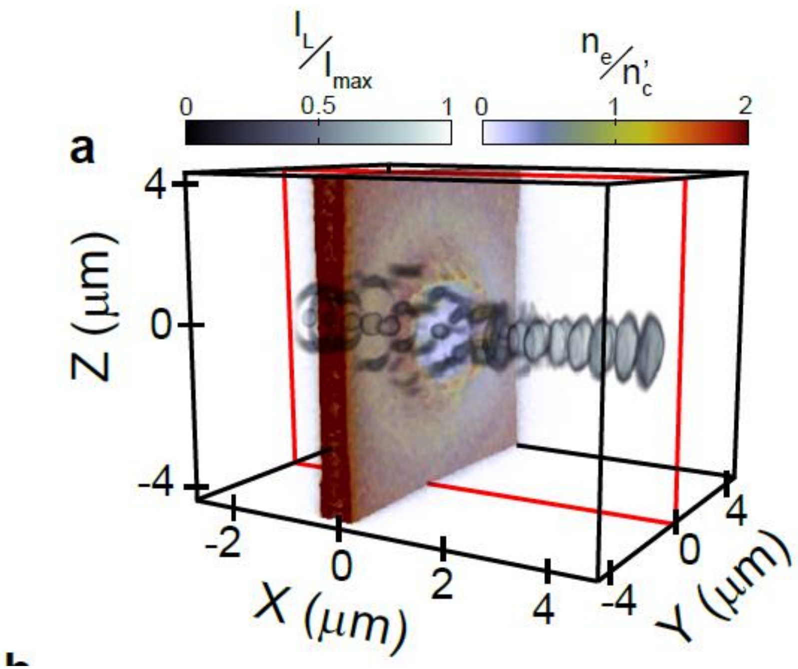

Temporal evolution of plasma aperture:

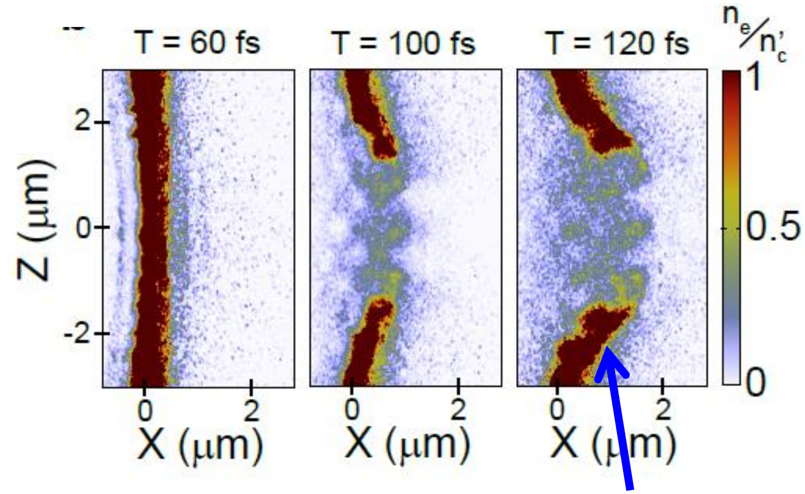

Deformation due to radiation pressure

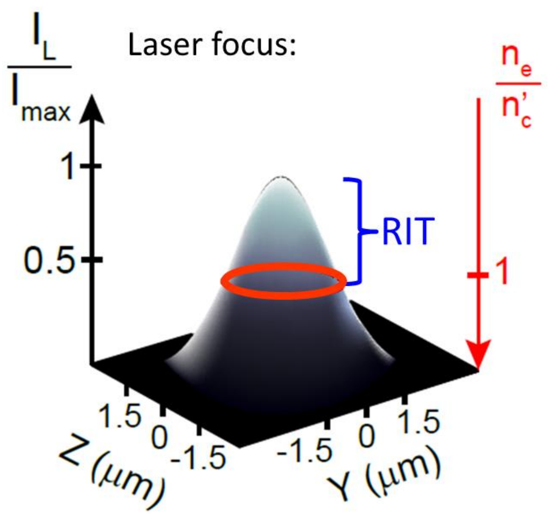

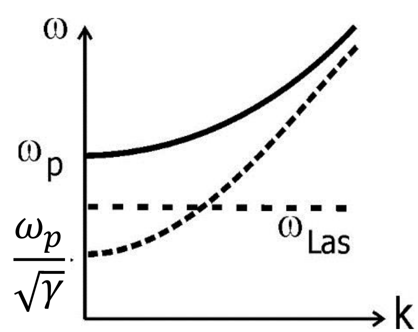

produces relativistically induced transparency over a diameter of a few times the laser wavelength

3D PIC simulations with a uniform planar target foil

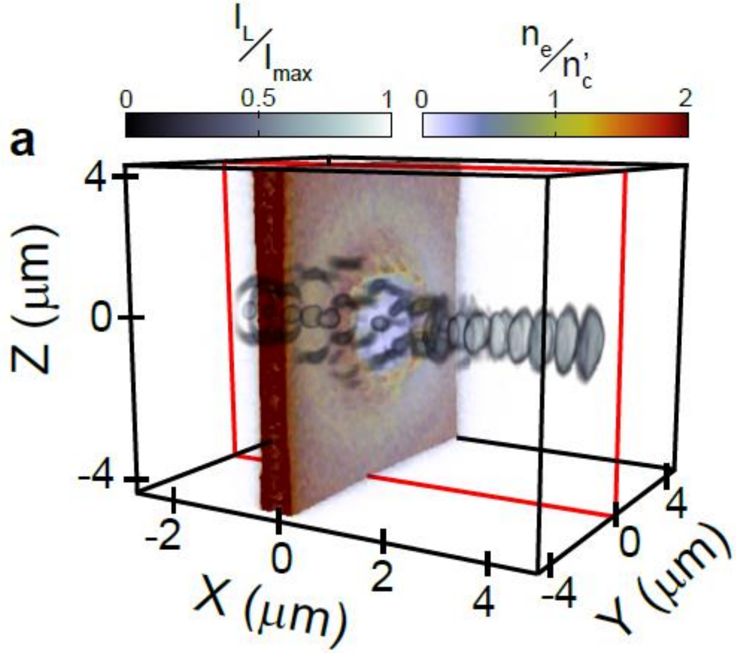

Temporal evolution of plasma aperture:

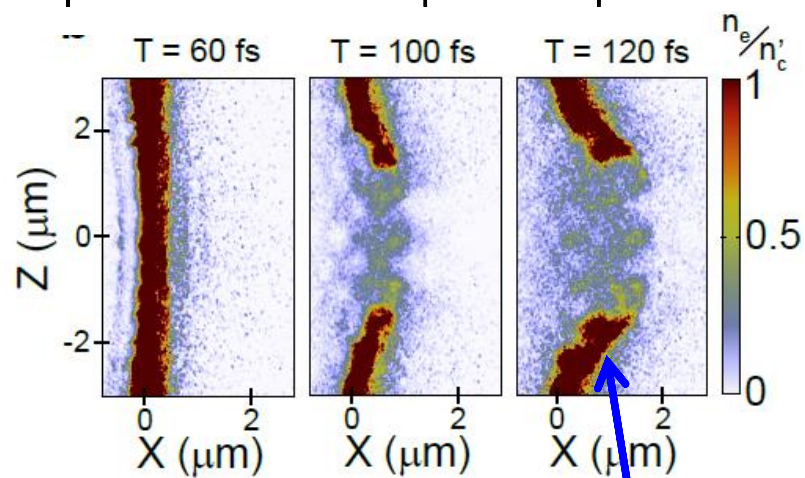

Deformation due to radiation pressure

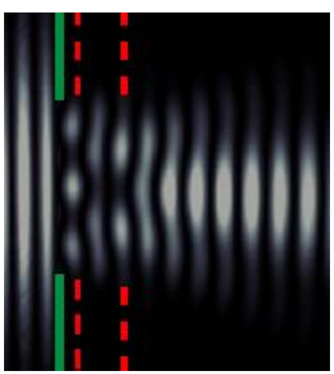

Hertz vector diffraction theory for a fixed aperture

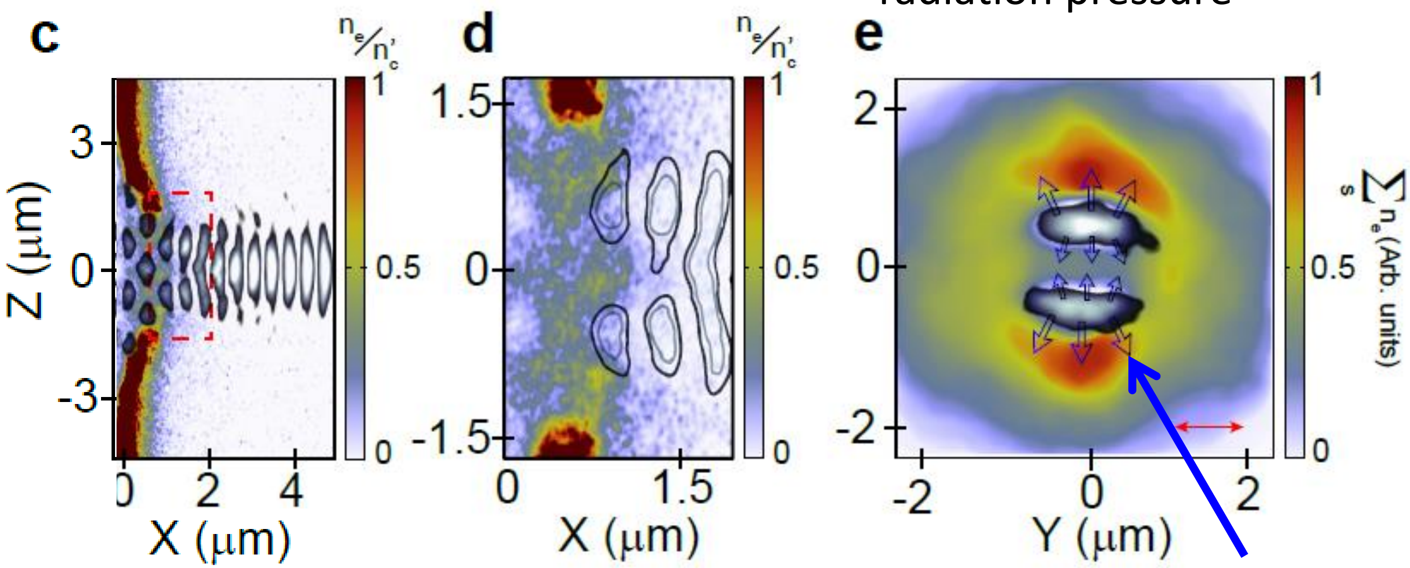

Ponderomotive expulsion

Influence of laser polarisation

Linear – fixed diffraction pattern

Circular – rotating pattern at constant velocity

Elliptical – variable velocity of rotation

angle of the polarization vector

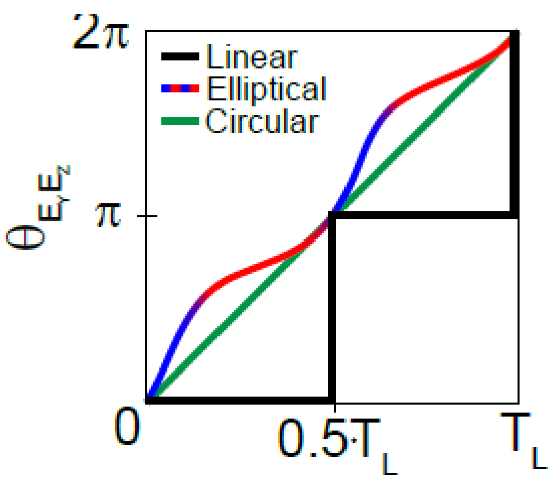

angular velocity of vector rotation

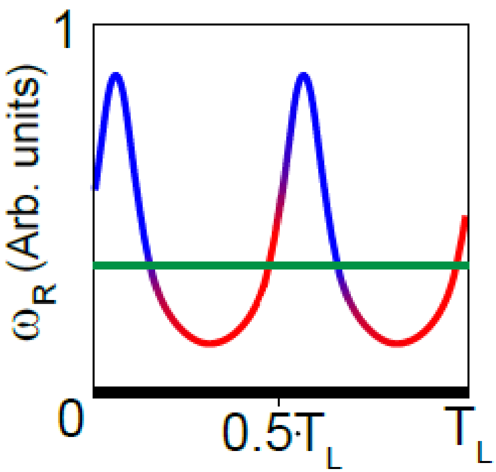

Circular

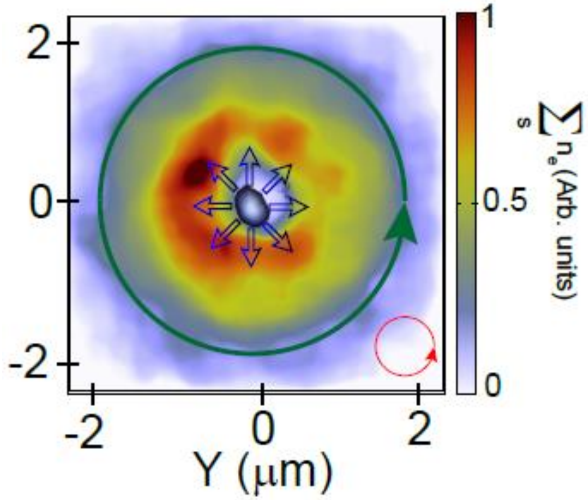

Elliptical

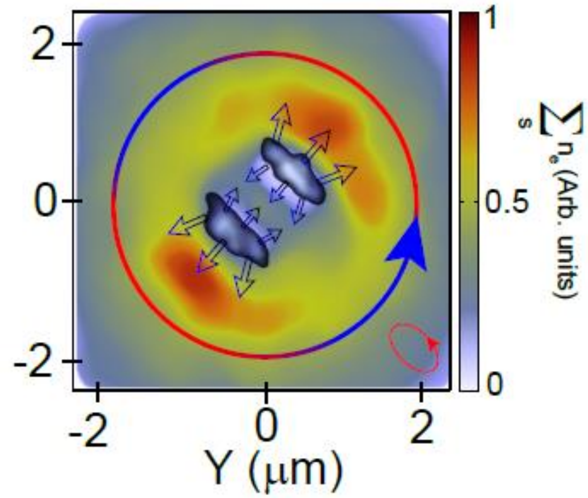

Gonzalez-Izquierdo et al, Nature Physics, 12, 505 (2016)

Influence of laser polarisation

Circular polarisation

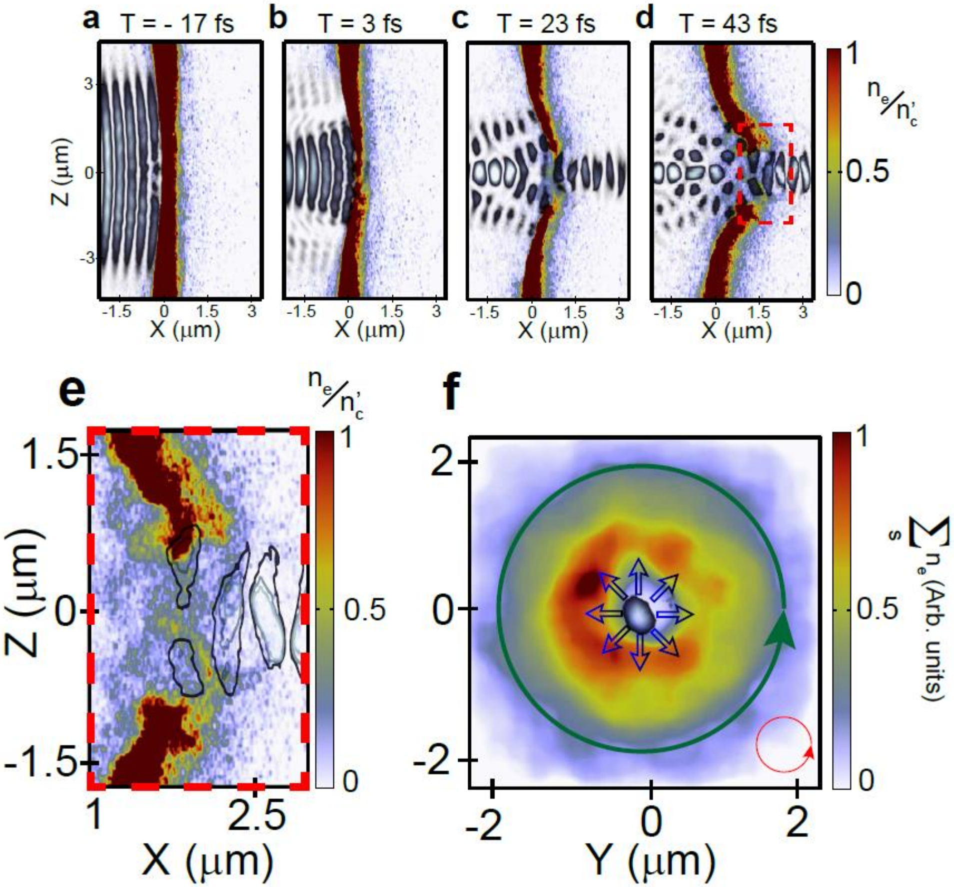

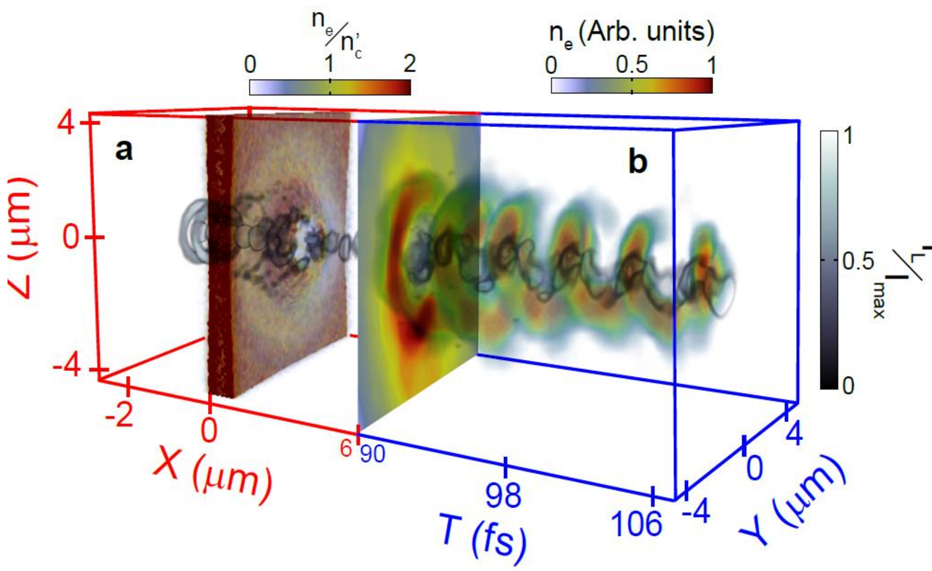

Gonzalez-Izquierdo et al, Nature Physics, 12, 505 (2016)

Comparison between experimental and simulations results

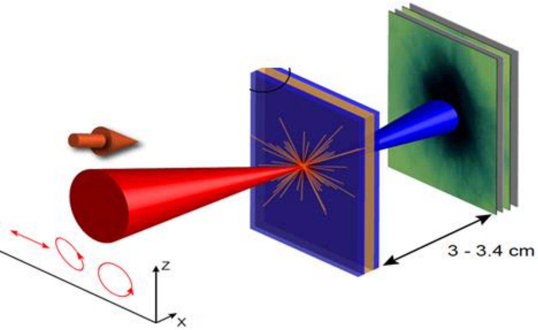

Experiment:

3D PIC simulation:

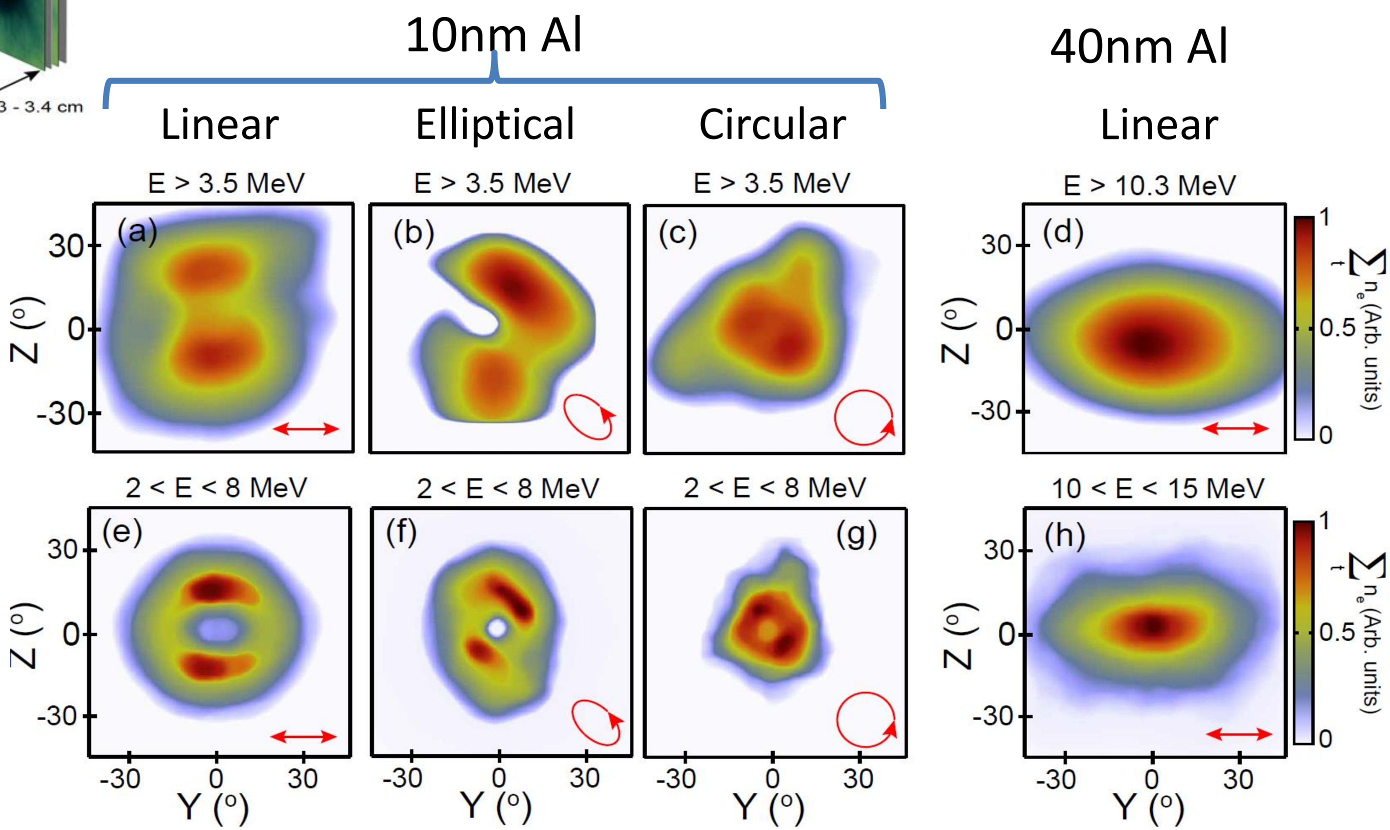

Gonzalez-Izquierdo et al, Nature Physics, 12, 505 (2016)

Influence on ion acceleration

Electron density structure mapped into the proton beam via modulation of the electrostatic field

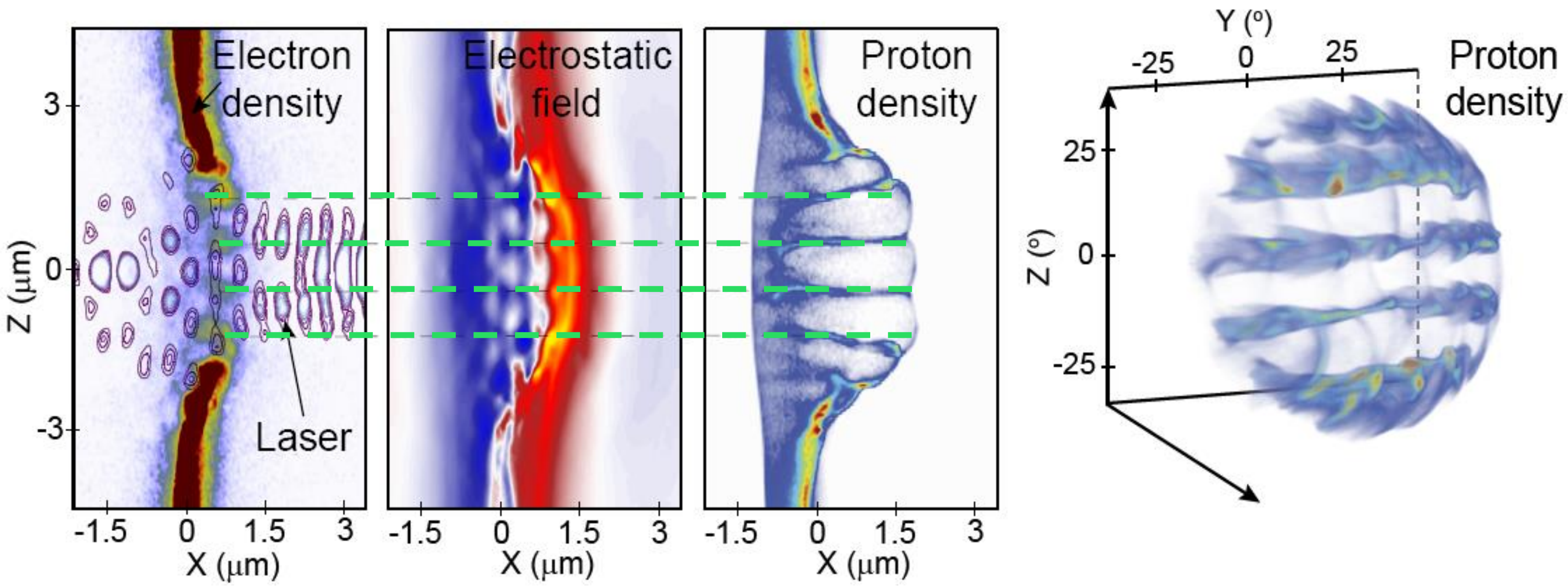

Gonzalez-Izquierdo et al., Nature Communications **7**, 12891 (2016)

Electron distribution maps into the protons via the electrostatic field

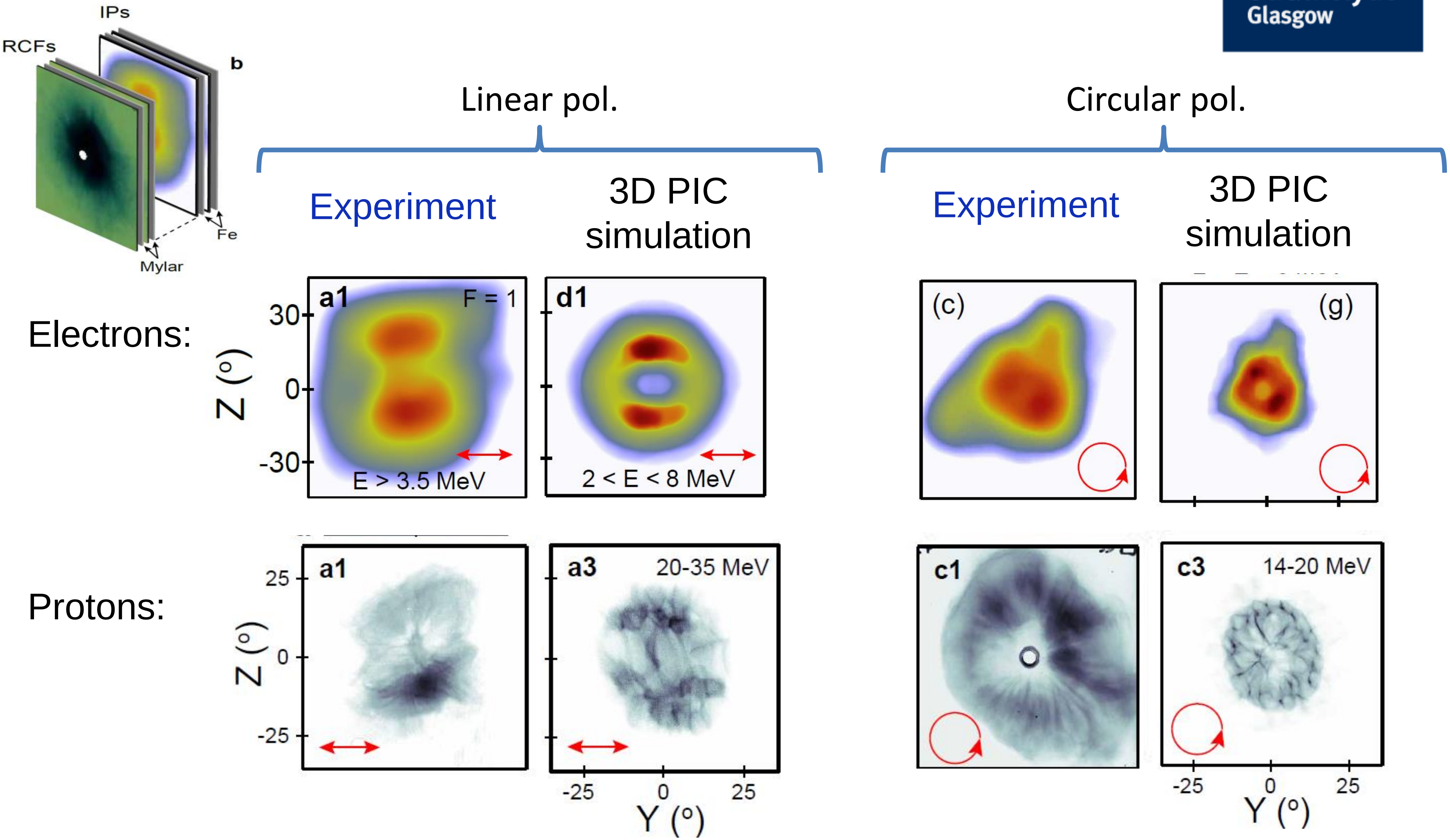

Gonzalez-Izquierdo et al., Nature Communications **7**, 12891 (2016)

Measurements of proton acceleration

Plasma mirror used to enhance the intensity contrast

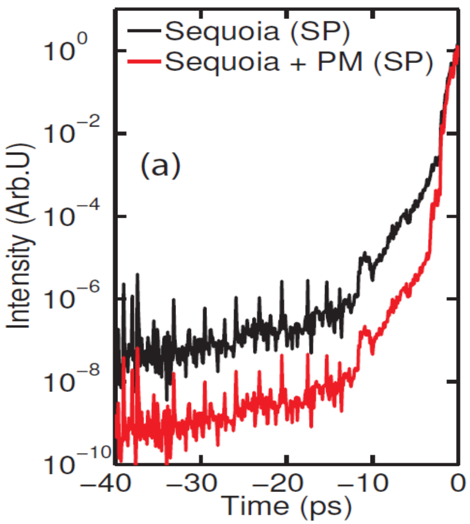

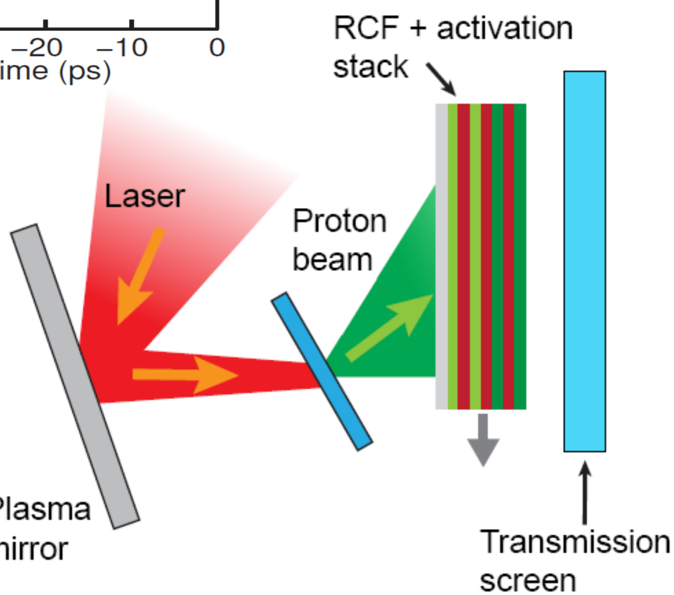

Stacked RCF dosimetry film measurements: $94<E_p<101$ MeV

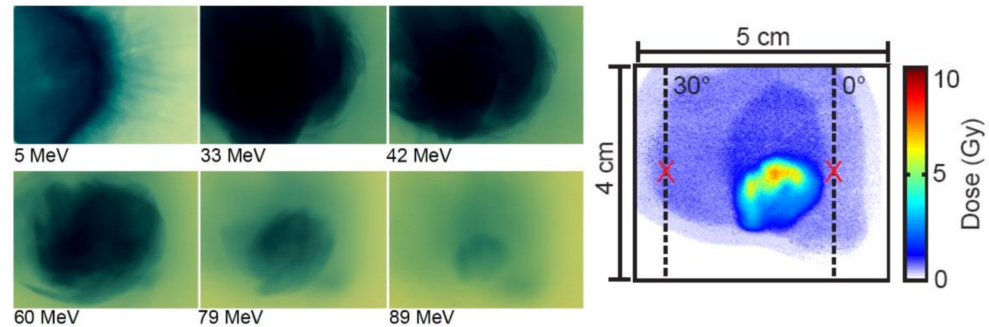

Nuclear activation measurements confirm proton energy >92 MeV

$^{63}Cu(p,n)^{63}Zn$

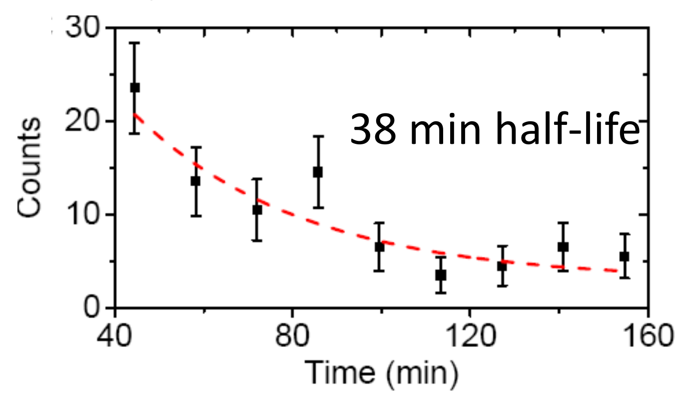

High proton energies obtained on Vulcan

Optimisation as a function of foil thickness has resulted in >95 MeV protons (between 94 MeV and 101 MeV)

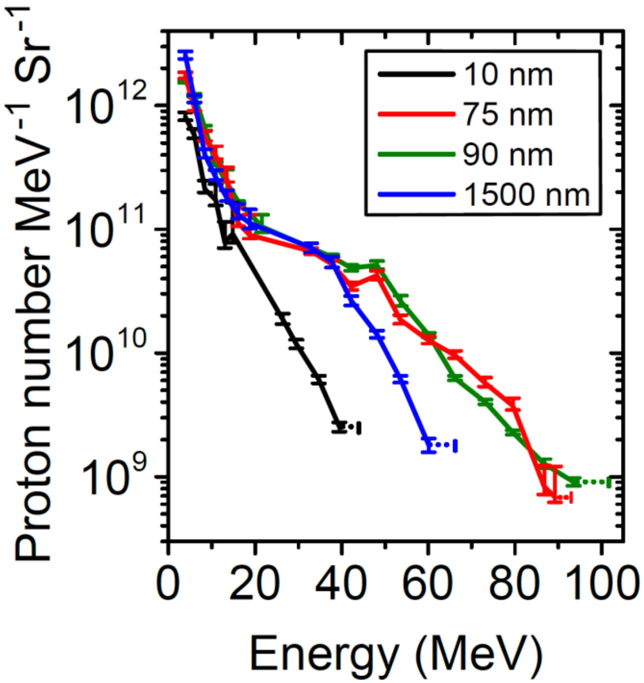

Higginson et al, Nature Communications, 9, 724 (2018)

High proton energies obtained on Vulcan

University of Strathclyde Glasgow

Optimisation as a function of foil thickness has resulted in
>95 MeV protons (between 94 MeV and 101 MeV)

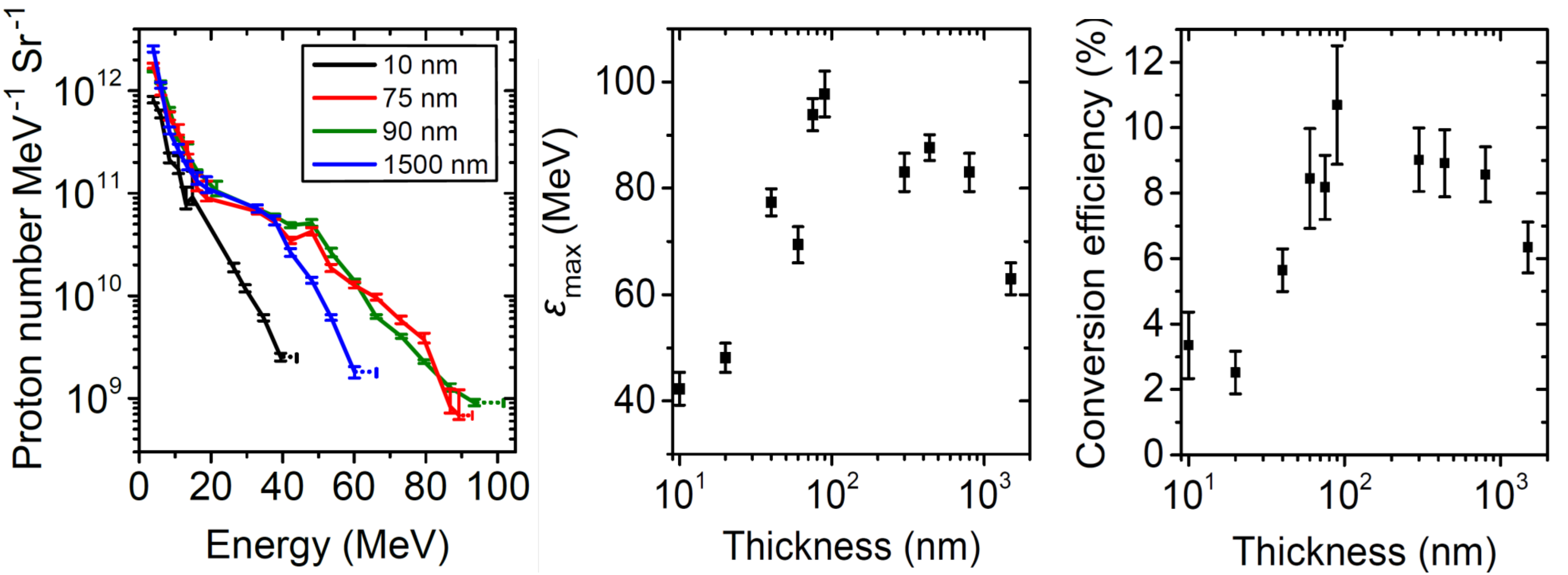

Higginson et al, Nature Communications, 9, 724 (2018)

High proton energies obtained on Vulcan

Correlated to measurements of critical surface velocity and transparency

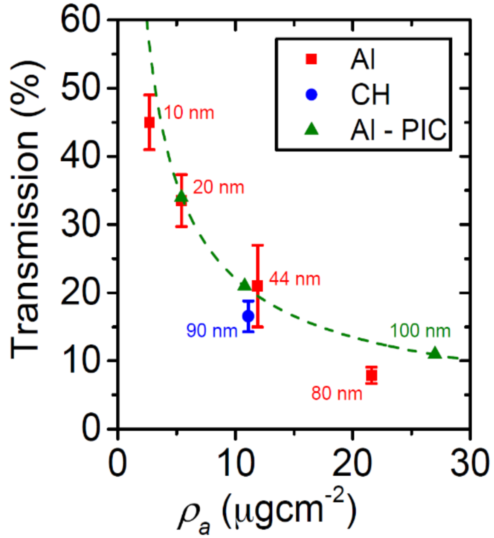

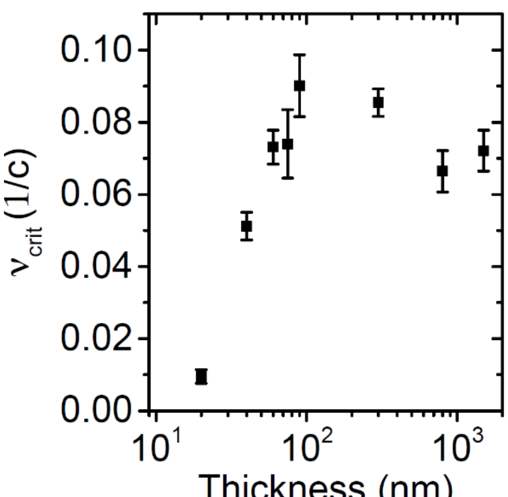

Optimisation as a function of foil thickness has resulted in >95 MeV protons (between 94 MeV and 101 MeV)

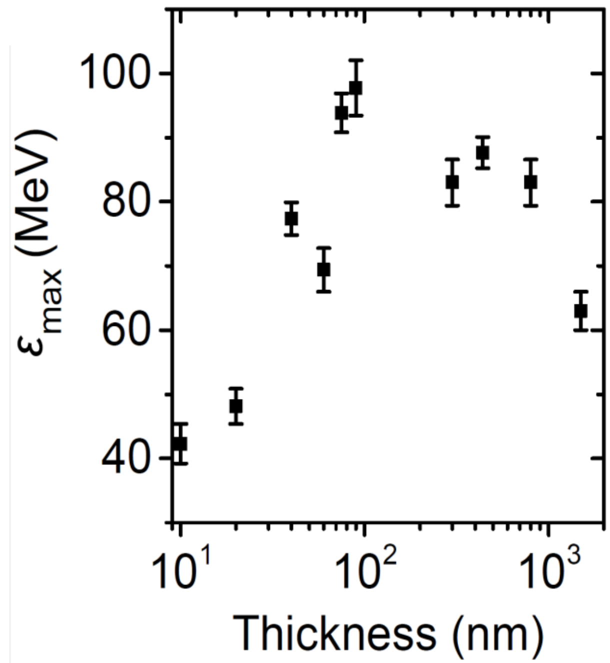

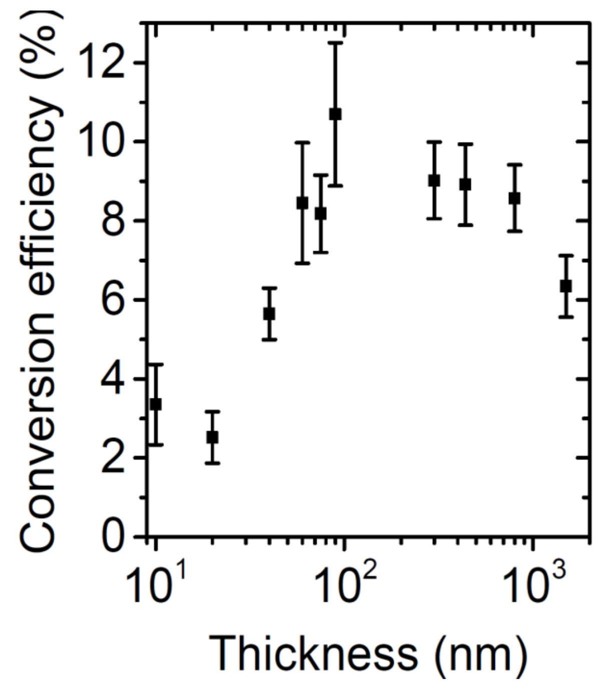

Higginson et al, Nature Communications, 9, 724 (2018)

Hybrid acceleration schemes

Linearly polarised laser results in a dual-peaked electrostatic field, produced by RPA and TNSA

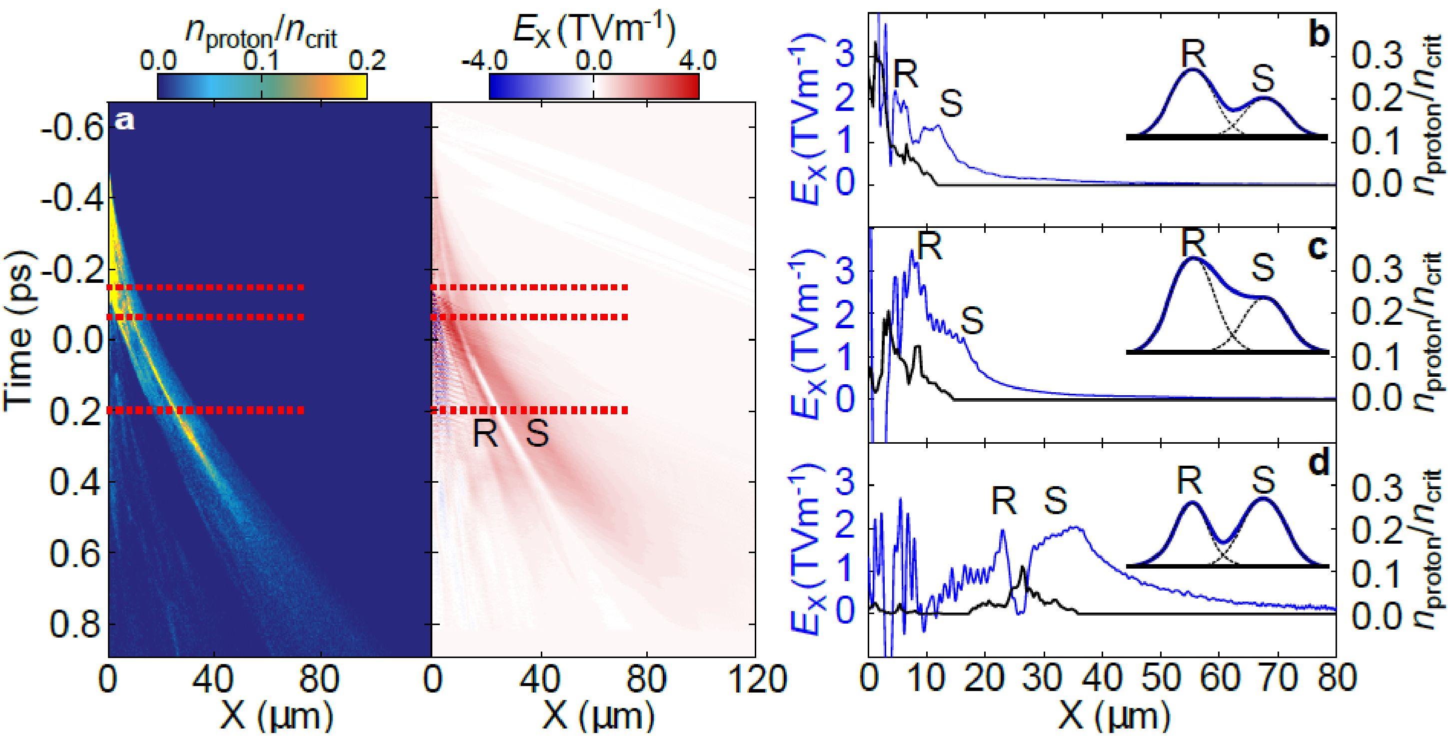

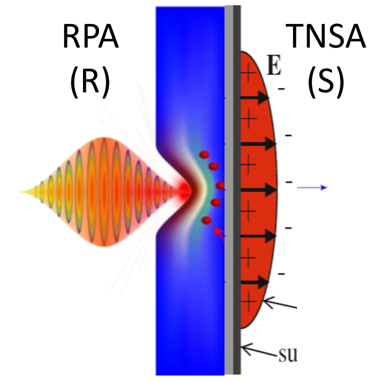

Laser pulse profile

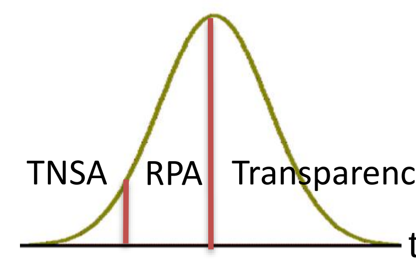

Higginson et al, Nature Communications, 9, 724 (2018)

Transparency-enhanced acceleration

Transmission of part of the laser pulse can enhance the TNSA field, by further heating the electrons, resulting in RIT-enhanced acceleration

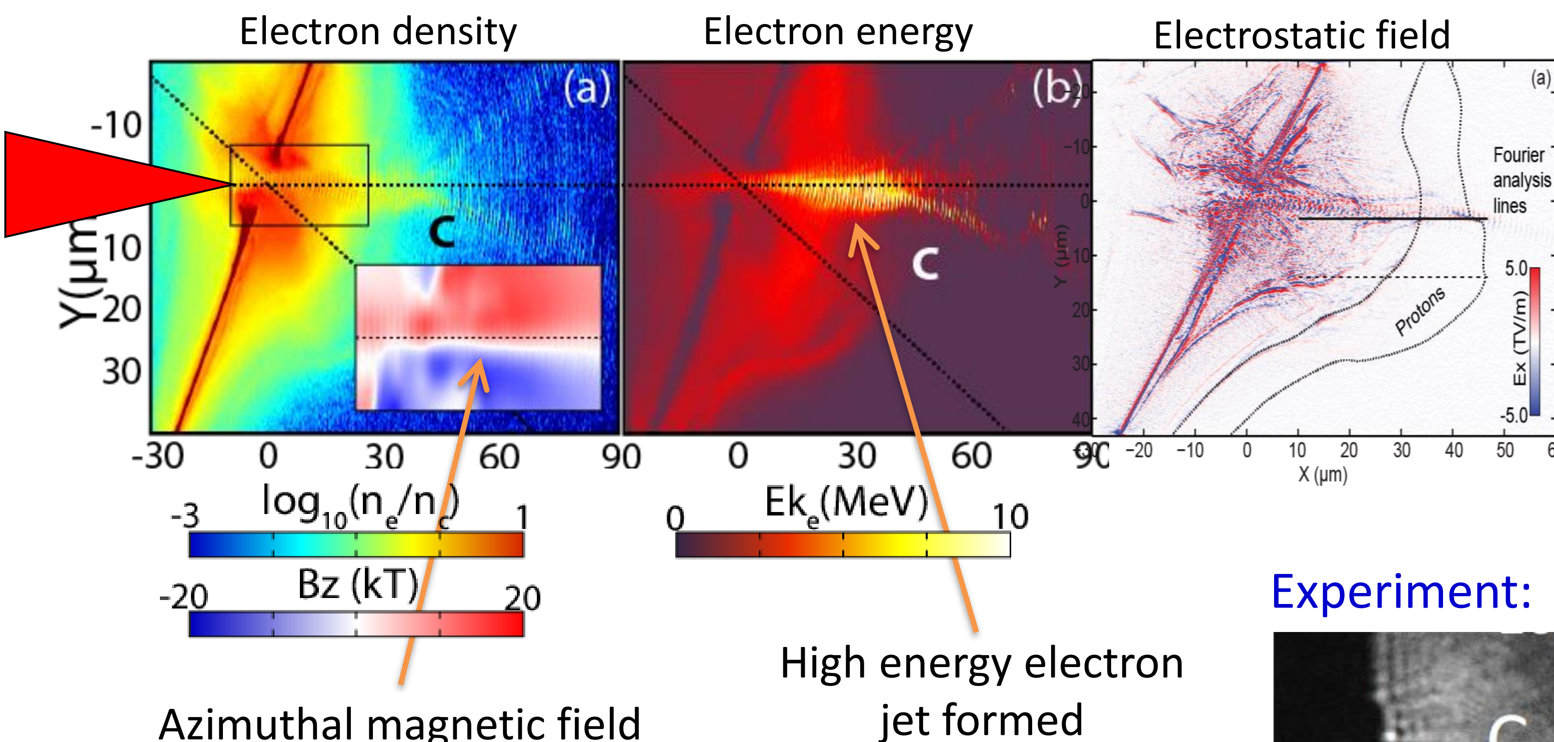

Experiment:

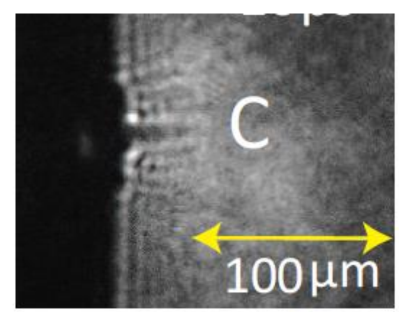

Powell et al, New J. Phys. 17, 103033 (2015)

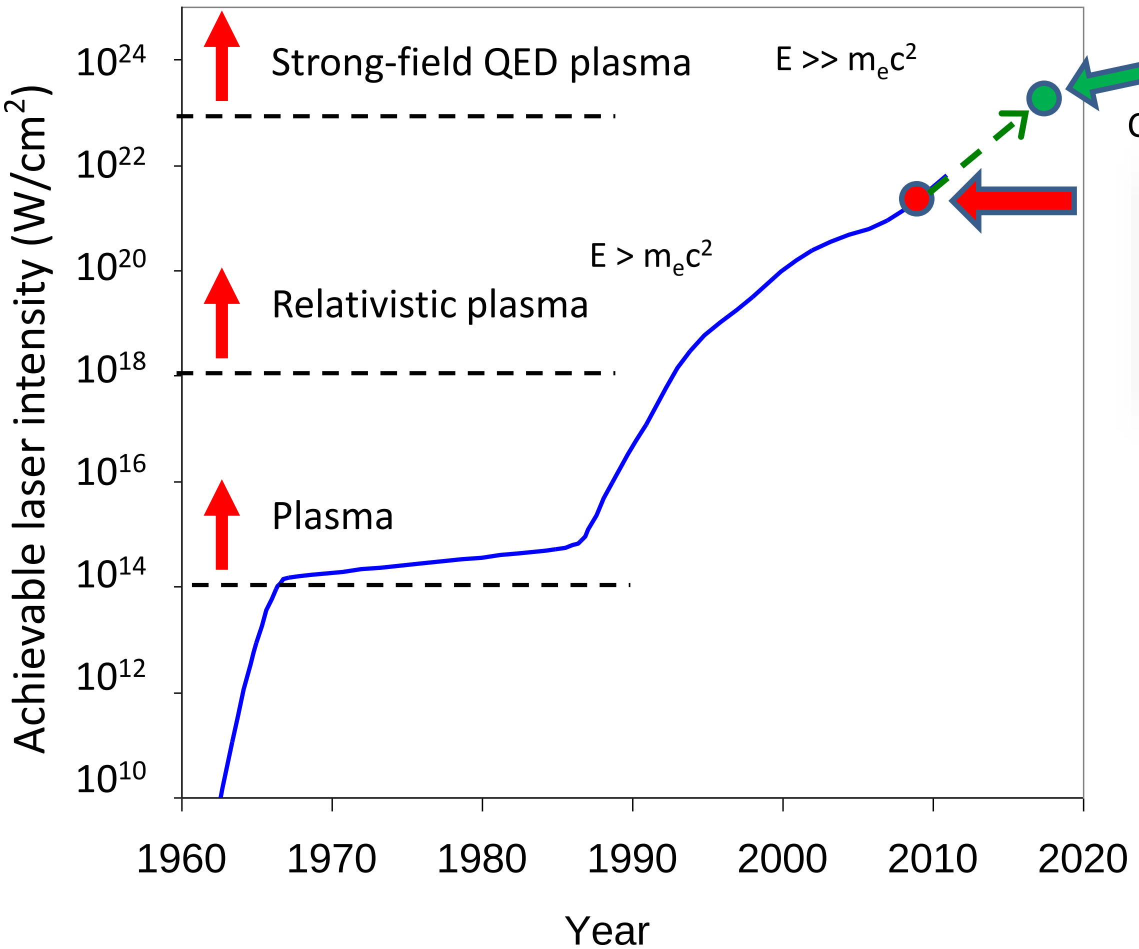

Extreme Light Infrastructure (ELI)

Central Laser Facility, RAL

Phelix, GSI

Scaling to multi-PW facilities: 10^{22} Wcm^{-2}

Linearly polarised laser light → Hybrid RPA-TNSA acceleration

RSIT onset τ_L=800 fs

Optimum for hybrid acc. τ_L=800 fs

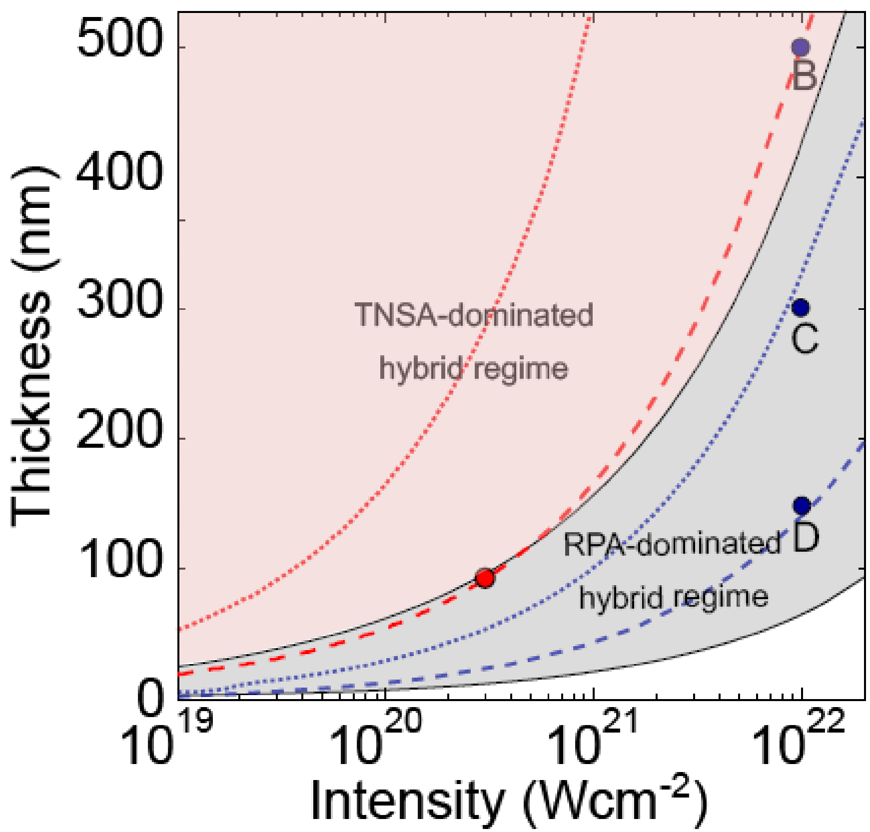

RSIT onset τ_L=40 fs

Optimum for hybrid acc. τ_L=40 fs

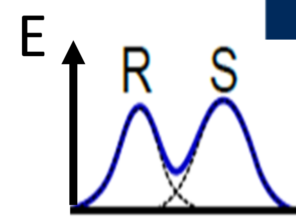

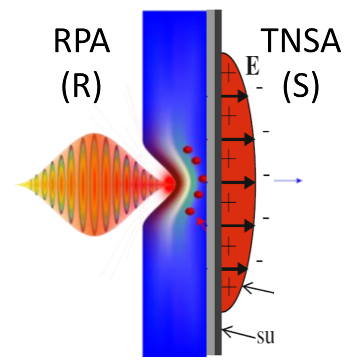

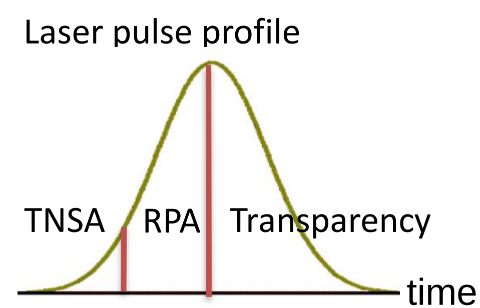

Limits for RPA-dominated hybrid regime calculated using the model in B. Qiao et al., Phys. Rev. Lett. 108, 115002 (2012)

Scaling to multi-PW facilities: 10^{22} Wcm^{-2}

Linearly polarised laser light → Hybrid RPA-TNSA acceleration

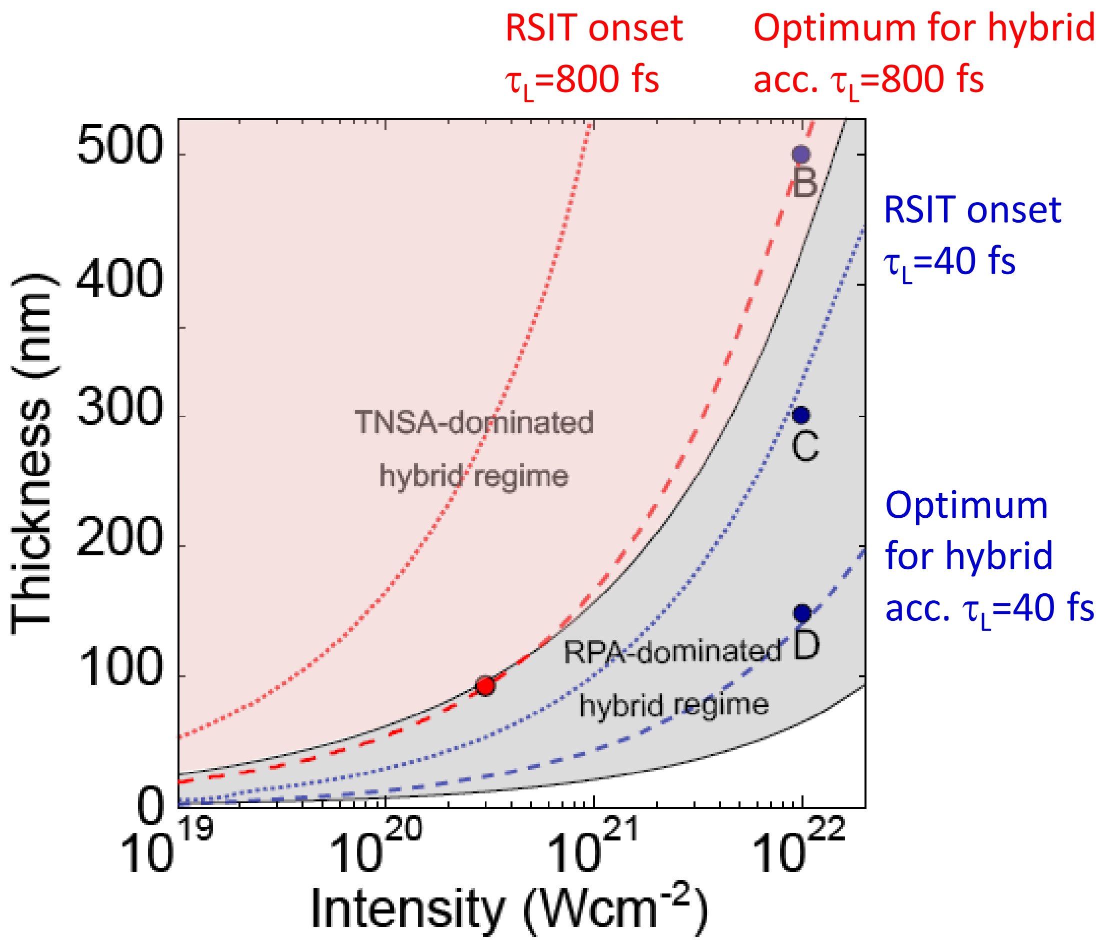

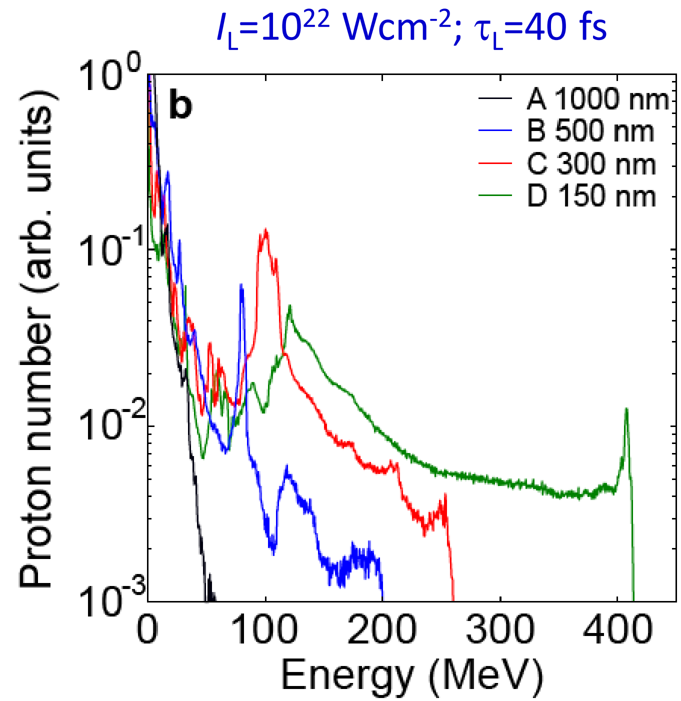

Tune thickness to get a spectral peak or enhance the maximum energy

Limits for RPA-dominated hybrid regime calculated using the model in B. Qiao et al., Phys. Rev. Lett. 108, 115002 (2012)

Summary points regarding ultrathin foil interactions

1. High contrast, short pulse intense laser interaction with ultrathin foil produces a relativistic plasma aperture, resulting in diffraction
2. The diffraction pattern and collective plasma response is strongly influenced by the degree of ellipticity in the laser polarization
3. Collective electron response is mapped into the proton beam spatial-intensity distribution
4. Near-100 MeV protons measured (with two diagnostics) using the Vulcan PW laser
5. Linearly polarised laser pulses drive a hybrid RPA-TNSA dual peaked electrostatic field acceleration scheme, enhanced by relativistic transparency occurring near the pulse peak
6. Hybrid acceleration scheme is scalable to next generation multi-PW lasers and offer new opportunities for ion beam control

Thank you for your attention!

References to ultrathin foil:

1. A. Higginson *et al*, Nature Communications, 9, 724 (2018)
2. B. Gonzalez-Izquierdo *et al.*, Applied Sciences. 1-18, (2018)
3. B. Gonzalez-Izquierdo *et al*, Nature Physics, 12, 505 (2016)
4. B. Gonzalez-Izquierdo *et al*, Nature Communications, 7, 12891 (2016)
5. B. Gonzalez-Izquierdo *et al*, High Power Laser Sci. Eng., 4, 33 (2016)
6. H. Powell *et al*, New J. Phys. 17, 103033 (2015)
7. M. King *et al*, Nuc. Instrum. Meth. A, 829, 163 (2016)
8. H. Padda *et al*, Phys. Plasmas, 23, 063116 (2016)

Acknowledgements:

- The staff at the Central Laser Facility, RAL and PHELIX group at GSI
- EPSRC and STFC research funding councils
- Laserlab-Europe

paul.mckenna@strath.ac.uk; GSI-22/05/2018